Univerzita Karlova

Přírodovědecká fakulta

Studijní program: Biologie

Studijní obor: Fyziologie živočichů

Bc. Zuzana Heřmanová

Úloha Aquaporin 4 kanálů a Transient Receptor Potential Vanilloid 4 kanálů při objemových změnách astrocytů

The Role of Aquaporin 4 channels and Transient Receptor Potential Vanilloid 4 channels in astrocytic swelling

Diplomová práce

Vedoucí diplomové práce: Ing. Miroslava Anděrová, CSc.

Praha, 2019

Prohlášení:

Prohlašuji, že jsem závěrečnou práci zpracovala samostatně a že jsem uvedla všechny použité informační zdroje a literaturu. Tato práce ani její část nebyla předložena k získání jiného nebo stejného akademického titulu.

V Praze, 25.4.2019

Podpis:

Poděkování:

Ráda bych poděkovala své školitelce Ing. Miroslavě Anděrové, CSc. za odborné vedení mé práce, za trpělivost a cenné rady. Také bych ráda poděkovala všem vědeckým pracovníkům a studentům, kteří mi umožnili zveřejnit výsledky uvedené v této práci jako součást odborných publikací. Tato práce byla financována Grantovou agenturou ČR, granty č. GACR 17-04034S, GACR 19-020463.

Abstract:

Astrocytes posses a wide range of functions within the brain. In response to ischemic conditions they swell due to increased uptake of osmolytes and they are mainly responsible for cytotoxic edema formation. However, they are also able to regulate their volume by releasing osmolytes together with water via the process of regulatory volume decrease (RVD). The Aquaporin 4 (AQP4) channel and Transient receptor potential vanilloid 4 (TRPV4) channel are suspected to be strongly involved in these processes of astrocytic volume regulation. The goal of the present diploma thesis was to clarify the role of both channels in astrocytic swelling *in situ*.

For our experiments we used a subpopulation of green fluorescent protein-labelled astrocytes from AQP4-deficient ($AQP4^{-/-}$), TRPV4-deficient ($TRPV4^{-/-}$) and control (Ctrl) mice. Cell volume alterations were induced in acute brain slices by hypoosmotic stress or by oxygen-glucose deprivation (OGD). Data were quantified using fluorescence intensity-based approach in the whole cells and in astrocytic endfeet.

Our results indicate, that there is no difference in astrocytic swelling or cell volume recovery between astrocytes from $AQP4^{-/-}$, $TRPV4^{-/-}$ and control mice when exposed to hypoosmotic stress. On the contrary, volume changes induced by OGD varied significantly between the experimental groups. Astrocytes from $AQP4^{-/-}$ mice showed only a weak increase in their volume in response to OGD, while they were unable to recover their volume when returned to normal arteficial cerebrospinal fluid (aCSF). Interestingly, the swelling of astrocytes from $TRPV4^{-/-}$ mice was comparable to that observed in controls. However, they were unable to recover their volume when returned to normal aCSF as observed in astrocytes from $AQP4^{-/-}$ mice.

Key words: Aquaporin 4, ischemia, Transient receptor potential vanilloid 4, water transport

Abstrakt:

Astrocyty mají v mozku celou řadu funkcí. V ischemických podmínkách zvětšují svůj objem v důsledku zvýšeného příjmu osmolytů a jsou tedy z velké části zodpovědné za rozvoj cytotoxického edému mozku. Jsou ale také schopné regulovat svůj objem uvolňováním osmolytů společně s vodou. Tento proces je nazýván regulované snižování buněčného objemu (RVD). Za kanály, které se regulace objemu astrocytů významně účastní, jsou považovány Aquaporin 4 (AQP4) a Transient receptor potential vanilloid 4 (TRPV4). Cílem této diplomové práce bylo objasnit úlohu obou těchto kanálů při objemových změnách astrocytů *in situ*.

Experimenty byly prováděny na populaci astrocytů, které byly značené zeleným flourescenčním proteinem a pocházely z AQP4-deficientních ($AQP4^{-/-}$), TRPV4-deficientních ($TRPV4^{-/-}$) a kontrolních (Ctrl) myší. Objemové změny byly vyvolány v mozkových řezech hypoosmotickým stresem a kyslíkovo-glukózovou deprivací (OGD). Data byla analyzována na základě změn intensity fluorescence v celých buňkách a v astrocytálních patkách.

Při aplikaci hypoosmotického stresu jsme mezi našimi experimentálními skupinami nenašli žádné rozdíly ve zvětšování objemu buněk nebo následném snižování buněčného objemu. Naopak objemové změny vyvolané aplikací OGD se mezi jednotlivými skupinami významně lišily. Astrocyty z $AQP4^{-/-}$ myší zvyšovaly svůj objem v reakci na OGD pouze mírně a po návratu do arteficiální cerebrospinální tekutiny (aCSF) nebyly schopné obnovit svůj původní objem. Astrocyty z $TRPV4^{-/-}$ myší měnily svůj objem stejným způsobem jako kontroly. Po návratu do aCSF nebyly nicméně schopné obnovit svůj původní objem, stejně jako buňky z $AQP4^{-/-}$ myší.

Klíčová slova: Aquaporin 4, ischemie, Transient receptor potential vanilloid 4, transport vody

Contents

Abbreviations

2D – two dimensional

3D – three dimensional

AA – Arachidonic acid

aCSF – Arteficial cerebrospinal fluid

ALDH1L1 – Aldehyde dehydrogenase 1 family, member L1

AQP4 – Aquaporin 4

AQP4e – Isoforme of Aquaporin 4

$AQP4^{-/-}$ – AQP4-deficient mice

α-Syn – α-Syntrophin

BBB – Blood brain barrier

BDNF – Brain-derived neurotrophic factor

BK – Big potassium channel

Ca^{2+} – Calcium cation

$[Ca^{2+}]_i$ – Intracellular concentration of calcium cations

$CaCl_2$ – Calcium chloride

Calcein-AM – Calcein-acethomethyl

CHIP28 – Integral membrane protein of red blood cells, later renamed Aquaporin

ClC-2 – Chloride channels type 2S

CNS – Central nervous system

Ctrl – Control

Cx30, Cx43 – Connexin 30, Connexin 43

EAAT – Excitatory amino acid transporter

ECS – Extracellular space

EETs – Eicosanoid metabolites

EGFP – Enhanced green fluorescent protein

FI – Fluorescence intensity

Fig. – Figure

GFAP – Glial fibrillary acidic protein

HT – High temperature (32°C)

Hypo – Hypotonic solution

IgG – Immunoglobulin G

K^+ – Potassium cation

KCl – Potassium chloride

Kir4.1 – Inwardly rectifying potassium channel 4.1

M1, M23, Mz – Isoformes of Aquaporin 4

MCAO – Middle cerebral artery occlusion

$MgCl_2$ – Magnesium chloride

Na^+ – Sodium cation

$[Na^+]_i$ – Intracellular concentration of sodium cations

Na_2HPO_4 – Sodium phosphate dibasic

$NaHCO_3$ – Sodium bicarbonate

NG2 – Nerve/glial antigen 2

NGF – Nerve growth factor

NKCC1 – $Na^+/K^+/Cl^-$-cotransporter type 1

NMDG-Cl – N-methyl-D-glucamine chloride

NMDA – N-methyl-D-aspartate

NMO – Neuromyelitis optica

NVC – Neurovascular coupling

OAP – Orthogonal array of particles

OGD – Oxygen glucose deprivation

OPC – Oligodendrocyte progenitor cell

PIP_2 – Phosphatidylinositol-4,5-bisphosphate

PLA2 – Phospholipase A2

PNS – Periferal nervous system

RT – Room temperature (23°C)

RVD – Regulatory volume decrease

SEM – Standard error of the mean

SUR1 – Sulfonylurea receptor 1

Tab. – Table

TRP – Transient receptor potential

TRPM4 – Transient receptor potential melastatin 4

TRPV4 – Transient receptor potential vanilloid 4

$TRPV4^{-/-}$ – TRPV4-deficient mice

VRAC/LRRC8 – Volume regulated anion channels

Wash – Washout

Z-stack – Set of focal images

1 Introduction

Ischemic brain injury is a leading cause of death and adult disability worldwide, moreover it is also well described in infants as a cause of neurological morbidity. Ischemic brain injury results from tromboembolic occlusion of a major cerebral artery or its branches, from a traumatic brain injury, cardiac arrest or even tumor growth/formation. So far, there is no reliable treatment for patients suffering from ischemic brain injury, therefore, numerous research projects are focused on elucidating the pathological mechanisms and identifying new drug targets in order to improve patient‘s outcome. Cerebral ischemia and trauma, as well as brain tumors, are accompanied by the development of brain edema, which represents a severe complication of above listed CNS disorders.

For decades, the researchers were mostly interested in rescuing damaged neurons, for example by targeting neuronal receptors, such as N-methyl-D-aspartate receptors. Currently, their attention turned towards glial cells, namely astrocytes, as these cells provide numerous essential functions, such as maintenance of ionic and neurostransmitter homeostasis, water transport, pH regulation, energy supply for neurons and even local blood flow regulation (Sofroniew and Vinters, 2010).

Under pathological conditions astrocytes markedly take up ions and neurotransmitters together with water, which results in an increase in astrocytic volume and therefore, these cells represent the main contribution to the development of brain edema. On the other hand, astrocytes are able to regulate their swelling by releasing osmotically active substances together with water, in the process termed regulatory volume decrease (RVD).

The aquaporin 4 (AQP4) channel and transient receptor potential vanilloid 4 (TRPV4) channel promptly respond to changed osmotic conditions within the brain tissue. Both AQP4 and TRPV4 channels are expressed on astrocyte membranes, and the recent findings suggest that these channels might represent possible targets for treating post-ischemic or post-traumatic edema formation. In addition, the involvement of AQP4 and TRPV4 channels in RVD was proposed in several studies (Benfenati *et al.*, 2011; Jo *et al.*, 2015; Iuso and Križaj, 2016).

The goal of the present diploma theses is to clarify the role of both channels in astrocytes *in situ* and compare the results with already known facts about their role in the cell volume regulation in cultured cells.

2 Ischemic brain injury

In general, ischemia is a cellular depletion of energy substrates (oxygen and glucose mainly), which leads to ionic-pump failure and to the disruption of ionic homeostasis (Schuier and Hossmann, 1980; Rosenberg, 1999). The lack of oxygen activates anaerobic metabolism pathways and lactate builds up, which decreases cellular pH. That - together with energy depletion - disturbs cellular osmoregulation, which is highly dependent on Na^+/K^+ ATPase and proton-dependent cotransport systems, and leads to the massive influx of water into the cells. These processes result in brain edema formation (Klatzo, 1987; Rosenberg, 1999).

Brain edema is defined as an abnormal water accumulation within the brain parenchyma, which causes an enlargement of the affected tissue and an increase in intracranial pressure (Klatzo, 1987, 1994). Besides ischemic injury, brain edema accompanies a wide range of brain and body pathologies, such as traumatic brain injuries, meningitis or hepatic encephalopathy (Ransom and Blank, 1975; Klatzo, 1987). It can be localized, thus affecting only a part of the brain, or generalized and spread through the whole brain parenchyma (Ransom and Blank, 1975). In the case of ischemia, the brain water content is already increased within an hour after the ischemic attack. However, it continuously increases for about 24 hours, when it reaches its peak, and then it starts to decline slowly (Hatashita, Hoff and Salamat, 1988). Under physiological conditions brain tissue is hyperosmolar when compared to blood plasma, while during ischemic brain injury the osmolarity differences rise significantly, which leads to massive water influx to the brain parenchyma (Hatashita, Hoff and Salamat, 1988).

Historically, the concept of two brain edema types was established. The vasogenic type, which is characterized by a blood-brain barrier (BBB) breakdown and an increase in its permeability. During this process water enters the brain an accumulates in extracellular space.

That causes its enlargement and results in compression of the cells in the affected area. The second type is cytotoxic edema and in contrast to the vasogenic type, it is characterized by water accumulation within the cellular elements of the brain parenchyma and leads to the shrinkage of the extracellular space (Ransom and Blank, 1975; Klatzo, 1994). Evidence showed that it is often the brain edema, which causes the fatal outcome of brain damage and that it is both, the cytotoxic and the vasogenic type of edema that play a key role in the severity of ischemic brain damage.

2.1 Cellular death

The process of hypoxic-ischemic injury is accompanied by an inflammatory and neurodegenerative response of the brain tissue, which leads to the death of brain cellular elements (Northington et al., 2001). Ischemia-induced cell death was described mostly on neuronal cells, where the neurodegenerative processes following ischemic injury occurr mainly by programmed cell death (apoptosis), necrosis, autophagy and excitotoxicity (or combination of those) (Linnik et al., 1993; Cheng et al., 1998; reviewed in Northington, Chavez-Valdez and Martin, 2011). The particular mechanisms of cell death - described in neonatal ischemic injury - are time distinguished. At the early phase, the necrosis takes place, followed by a delayed phase of apoptosis and inflammation with a secondary phase of necrosis (Northington et al., 2001; Carloni et al., 2007). It is also suggested that the necrotic death of a certain group of neurons can result in the death of other connected cells (Northington et al., 2001).

The synapses between neurons enable cell communication, but can also represent the trigger for damaging processes, in general called the excitotoxicity. In a healthy brain, the excitatory synaptic transmission is mediated mostly by glutamate. In case of ischemia (or another brain damage), the glutamate release can cause excessive neuronal activation, which leads to cytotoxic cellular swelling, degeneration of cell compartments and to the death and phagocytosis of the cells (Olney, Ho and Rhee, 1971; Choi, 1988). During ischemia, the glutamate is extensively released from synaptic terminals in response to excessive stimulation. It is released into the extracellular space, from where it is cleared by astrocytes. The pool of glutamate in ischemic glia is increased by about 60 %, compared to the physiological levels (Torp et al., 1991). However, glutamate does not remain in astrocytes. Under ischemic conditions, the glutamate transporters on astrocytic membranes reverse their

function and glutamate is released back into the extracellular space, where it further affects neuronal functions (Rossi, Oshima and Attwell, 2000).

Glutamate opens ion channels in neuronal membranes and allows sodium cations (Na^+) to enter the cells. In healthy brain the Na^+ is removed from the cells by Na^+/K^+ ATPase, while during ischemia, when the neuronal depolarization is repetitive and continuous, the intracellular concentration of sodium $[Na^+]_i$ increases above physiological levels and is followed by a massive influx of water, which leads to cellular swelling (Olney et al., 1986). In ischemic brain, extracellular glutamate causes long-term depolarization of neurons that interrupts local cerebral functions and results in an enlargement of infarct lesion (Mies, Iijima and Hossmann, 1993; Dijkhuizen et al., 1999). These changes are more prominent in the lesion core, where the depolarization is irreversible. On the contrary, on the border zones of the lesion (in penumbra) the changes caused by depolarization, as well as depolarization itself, can be transient (Dijkhuizen et al., 1999). The cellular swelling and damage mediated by Na^+ is strengthened by an increased influx of calcium cations (Ca^{2+}) (Berdichevsky et al., 1983) and the same effect can also be caused by glutamate analogs, such as aspartic acid or kainate, and increased levels of extracellular potassium cations (K^+) (Olney, Ho and Rhee, 1971; Berdichevsky et al., 1983; Busch et al., 1996).

2.2 Models of Ischemia

Ischemia is intensively studied using *in vitro* and *in vivo* models. Each model has its advantages and shortcomings, but altogether they are useful tools for studying and mimicking human pathologies. *In vitro* models (cell cultures) hold many possibilities, because they can vary in cell type and in the animal species, they are prepared from and they are usually used for studying molecular events during ischemia. Primary cultures are most often isolated from mice or rats, but can also originate from bovine brain or primates. Another option for *in vitro* models of ischemia are immortalized cell lines originating from variable organisms and cell types. These models can include single cell type (monoculture) or more cell types that are co-cultured together in the same conditions (reviewed in Tornabene and Brodin, 2016). Often used *in vitro* treatment is oxygen-glucose deprivation (OGD), which is employed in order to mimic the disruption of oxygen and nutrients supply to the brain. In OGD, the cells are cultivated in glucose-free media in an atmosphere of zero or low (5 – 7 %) oxygen. This exposure can last from about 15 minutes to more than a day. The OGD can be performed also

on acute brain slices, which more likely resemble pathophysiology of living animals (Tasca, Dal-Cim and Cimarosti, 2015).

Animal models of ischemia relatively closely simulate human pathology, although in human brain the ischemic injury has different manifestation, localization, cause and outcome in every patient. These models can be provided on genetically modified animals, and thus help researchers to understand the roles of different proteins and molecules in a proper context in pathological situations *in vivo*.

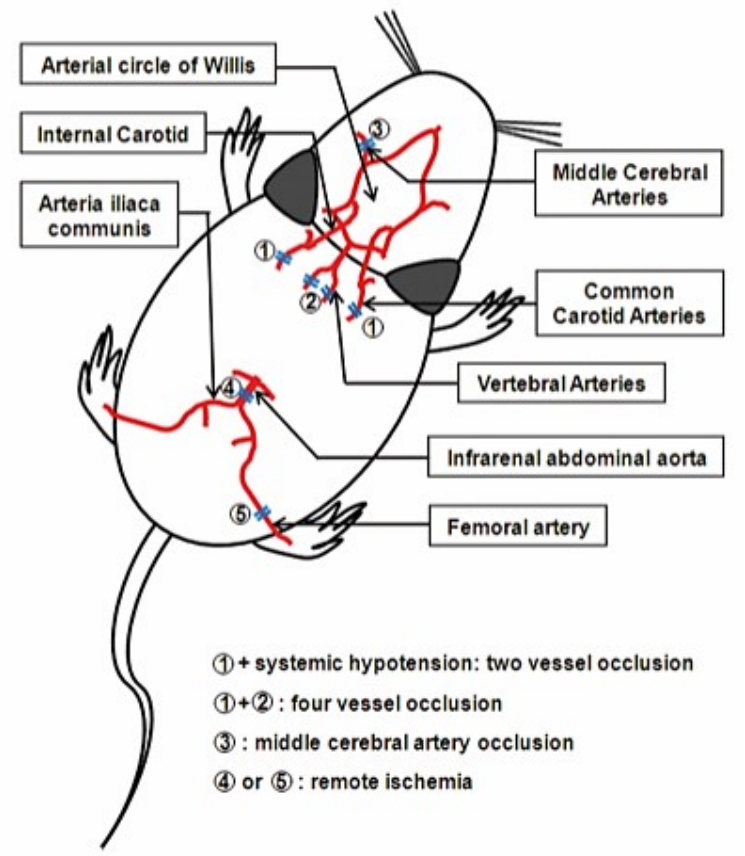

Figure 1: Rodent models of ischemia. 1. Brief occlusion of the bilateral common carotid arteries combined with either vertebral artery coagulation (four-vessel occlusion, ①+②); 2. Brief occlusion of the bilateral common carotid arteries with systemic hypotension (two-vessel occlusiov, ① +systemic hypotension); 3. Brief occlusion of one middle cerebral artery (MCAO, ③); 4. Occlusion of unilateral femoral artery or the infrarenal abdominal aorta (remote ischemia, ④ or ⑤). Taken from: Stelter et al., 2014

In vivo, we distinguish two types of cerebral ischemia, focal or global. In focal ischemia, the blood flow is reduced only in a distinct region of the brain, whereas in the global ischemia the blood flow is reduced in the entire brain (reviewed in Bacigaluppi, Comi and Hermann, 2010). As mentioned above, most of the ischemic injuries result from occlusion of a major brain vessel or its branches (mostly of the middle cerebral artery, Fig. 1). For this reason, the middle cerebral artery occlusion (MCAO) model was developed (reviewed in Fluri, Schuhmann and Kleinschnitz, 2015). It is a highly reproducible method of standardized experimental stroke, which is usually performed on mice or rats, but using larger animals, such as primates, is also possible (reviewed in Durukan and Tatlisumak, 2007). MCAO is a typical model of focal ischemia. The occlusion can be transient, and allow reperfusion, or permanent (Kaneko, Nakamura and Ogawa, 1985; reviewed in Liu and McCullough, 2011). In the transient MCAO, the vessel is blocked, so it would not allow any blood flow, for a defined period on time (hours mostly) and then the blockage is removed and the nervous tissue is reperfused. In the permanent MCAO models, the vessel remains occluded through the entire experiment, without the reperfusion phase (reviewed in Liu and McCullough, 2011 and Woodruff et al., 2011).

Another possible approach is using global models of ischemia. In the past, these models were suspected to have much lesser clinical significance, compared to the focal approaches. However, currently the global models of ischemia are considered to be of great clinical relevance, especially to pathologies, such as cardiac arrest or asphyxia (McBean and Kelly, 1998). In experimental animals, global ischemia is usually induced by multiple vessel occlusion, typically both carotids (two-vessel occlusion, Fig. 1) or carotids and vertebral arteries (four-vessel occlusion, Fig. 1). Complete global ischemia can be achieved by neck-cuff, cardiac arrest or – without the possibility of reperfusion – by decapitation (reviewed in Woodruff et al., 2011).

3 Glial cells

Glial cells are also called neuroglia or simply glia. During history, glial cells were described as ‚helper' cells for the neurons, with just basic functions and no role in neural system development or diseases. However, with the progress of technology and science, the view on glial cells changed. Today, glial cells comprise a population of non-neuronal cells in the central and peripheral nervous system (CNS and PNS) that occupy about a half of the brain / spinal cord volume and play a crucial role in CNS development, its normal, healthy functioning and in pathologies. The term ‚glial cells' describes a wide category, which

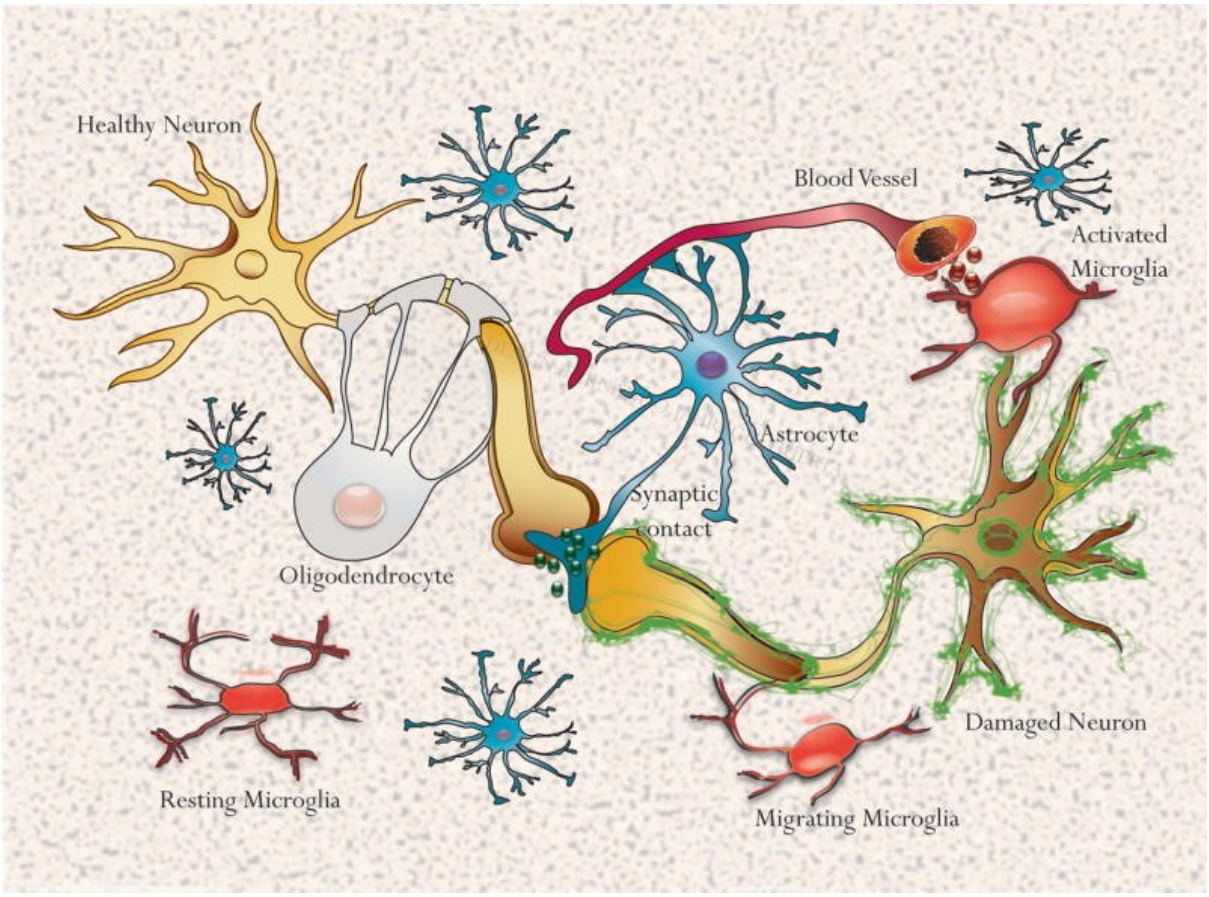

Figure 2: Glial cells in an adult brain. Astrocytes (blue) envelope synapses and make close contacts with blood vessels. Microglia (red) constantly screen brain tissue and answer to microenvironment changes by their activation and changes of morphology. Oligodendrocytes (gray) create myelin sheats around axons and accelerate neuronal communication. Taken from: Jeuregui-Huerta et al., 2010

contains several cell types with different and very specialized functions. In the PNS the main cell types are Schwann cells, which form myelin sheaths around axons, and amphicytes, small cells with short processes surrounding neuronal soma. In the CNS the situation of glial cells is more complicated because in CNS more types of glia can be found (reviewed in Jessen, 2004; Fig. 2).

3.1 Oligodendrocytes

Oligodendrocytes are myelinating cells of the CNS and make about 5 – 8 % of the glial population in a healthy brain. Oligodendrocytes differentiate from oligodendrocyte progenitor cells (OPCs). These arise from neural stem cells in specialized domains in a response to local factors, such as *Olig* proteins, and migrate to reach all parts of CNS, where these progenitors differentiate into mature oligodendrocytes (Yang, Lewis and Miller, 2011). Each oligodendrocyte envelopes a few axons in several layers of myelin coat. This increases the speed of axonal conductance as well as the efficiency of neural transmission. The number of myelin coats created by single oligodendrocyte is regulated by individual axons and their activity (Almeida *et al.*, 2011; Mensch *et al.*, 2015).

Thanks to the close contacts between oligodendrocytes and neurons a question arose, whether the oligodendrocytes couple with neurons or any other cell type. The coupling is quite common between CNS glial cells (especially astrocytes). Formation of gap junctions was proven between astrocytes and oligodendrocytes, which express three different types of connexin proteins. These are able to assemble into heterodimers with astrocytic connexins (Magnotti, Goodenough and Paul, 2011). Furthermore, the astrocyte – oligodendrocyte gap junctions are required for proper axonal myelination and their loss leads to myelin vacuolization (Tress *et al.*, 2012). Also, the oligodendrocytes in white matter are coupled and form a functional network. Some results even show, that the coupling between two oligodendrocytes is stronger than that between oligodendrocytes and astrocytes (Maglione *et al.*, 2010).

3.2 Microglia

Microglia are small glial cells with a large number of short branching processes. They are CNS macrophages with a wide range of functions in development, neuroinflammation, disease and brain injury. They comprise about 10 % of the glial population. Microglial

progenitors can be detected in early embryonic development and originate from the first wave of hemopoietic cells from a yolk sac (Alliot, Godin and Pessac, 1999; Ginhoux *et al.*, 2010). During development microglia at first accumulate in the white matter and they migrate to the gray matter in the later postnatal phases. In the ‚white matter phase', their morphology is amoeboid or they have a few thick processes (Ueno *et al.*, 2013). They also produce neurotrophic factors - proteins that regulate neuronal functions and survival. Microglia were shown to constitutively produce brain-derived neurotrophic factor (BDNF) and when stimulated, they also produce nerve growth factor (NGF) (Nakajima *et al.*, 2001; Ueno *et al.*, 2013). Via production of BDNF and NGF (and other factors), microglia play a key role in the developmental and adult brain plasticity. Recent studies have suggested, that microglia participate also in the processes of learning and memory by learning-induced remodeling of excitatory synapses (Pascual *et al.*, 2012; Parkhurst *et al.*, 2014).

Microglia are usually viewed as CNS resident macrophages. They survey their surrounding by moving their processes. Such motility of microglial processes is due to via rearrangement of actin filaments (Nimmerjahn, Kirchhoff and Helmchen, 2005). In response to pathological stimulation, microglia change their phenotype and transform from so-called ramified or resting cells (small cells with short processes) into an amoeboid phenotype. The amoeboid cells show enhanced motility and express sets of membrane receptors, which enable them to migrate to the sites of inflammation and infiltrate it soon after the brain injury. The migration is driven by proteins of complement and their receptors on the microglial surface (Nolte *et al.*, 1996). These cells are capable of phagocytosis and production of pro-inflammatory cytokines (Parakalan *et al.*, 2012) and also a production of glia-promoting factors - proteins, that stimulate astrocytes and support their transformation into a reactive state (Giulian and Baker, 1985).

3.3 NG2 glia

NG2 glia are a cell population, which is committed to the OPCs and also termed polydendrocytes. They exist in the white as well as grey matter, and they were found in developmental phases as well as in adulthood. They express transmembrane chondroitin sulfate proteoglycan named nerve/glial antigen 2 (NG2). NG2 glia are highly reactive cells, that play an important role in nerve injury (Dawson *et al.*, 2003).

NG2 cells are able to undergo dramatic changes and they proliferate and develop into oligodendrocytes and astrocytes. *In vitro*, these cells are capable of differentiating even into neurons, depending on the conditions (Kondo and Raff, 2000; Honsa *et al.*, 2016). *In vivo*, the results are rather contradictory. It was demonstrated that NG2 glia are able to differentiate into oligodendrocytes during the whole life span (Kang *et al.*, 2010; Huang *et al.*, 2014), while their differentiation into astrocytes *in vivo* was confirmed during development in prenatal stages (Huang *et al.*, 2014), and after ischemia, when NG2 cells increase their expression of glial fibrillary acidic protein (GFAP – astrocyte marker) and their phenotype change towards reactive astrocytes (Honsa *et al.*, 2016).

3.4 Astrocytes

Astrocytes (or astroglia) represent the largest population of glial cells within the brain and can be found in the entire brain parenchyma. The number of astrocytes varies between the species, as well as the ratio of astrocytes to neurons, which also differs among individual regions of the brain. In mammalian brains, astrocytes outnumber neurons for example in cortical regions, but they are outnumbered by neurons in the cerebellum (Herculano-Houzel, 2014).

Astrocytes display a specific and quite complicated morphology. On the basis of their morphology and distribution in CNS distinct types of astrocytes were identified (Miller and Raff, 1984). Fibrous astrocytes are localized mainly in the white matter. They have many long fiber-like processes which spread quite regularly. Contrarily, the protoplasmic astrocytes are localized in gray matter and typically posses fewer processes that are organized irregularly (Miller and Raff, 1984). Electron microscopic analyses showed that both types vary also in their contacts with neuronal cells. Whereas the processes of protoplasmic astrocytes surround synapses more often, the fibrous astrocytes contact nodes of Ranvier (Sofroniew and Vinters, 2010). In human and hominid brains, however, other specialized types were described: interlaminar and varicose projection astrocytes (Oberheim *et al.*, 2010). All four types identified in the human brain have their specific morphology. The varicose projection astrocytes have long processes with varicosities (spaced every 10 μm) which are straight with a small number of branches. The function of these branches is not known (Oberheim *et al.*, 2010). A relatively small number of these cells was found in the layers 5 and 6 of the cortex. Primate-specific interlaminar astrocytes localize strictly in the cortical

layer 1. They have an oblong soma and processes that extend to both, the pial surface and deeper layers of the brain (Oberheim *et al.*, 2010).

On a molecular basis, all astrocytes can be identified immunohistochemically by using antibodies against specific protein markers. The most frequently used is the glial fibrillary acidic protein (GFAP). It is an important structural protein and component of intermediate filaments in astrocytes, together with vimentin and nestin. GFAP is expressed in different isoforms and their localization varies in the brain regions and they also have distinct subcellular localization (Thomsen *et al.*, 2013). Recently, aldehyde dehydrogenase 1 family, member L1 (ALDH1L1) was identified as the new astroglial marker (Cahoy *et al.*, 2008). It is a folate enzyme that converts 10-formyltetrahydrofolate to tetrahydrofolate, playing an important role in many reactions like de novo nucleotide biosynthesis and the regeneration of methionine, thus having a major impact on cell division and growth (Krupenko, 2009).

3.4.1 Astrocyte functions

Astrocytes posses a wide range of functions, which differ in developing and in the adult brain. It was demonstrated that in developing brain astrocytes affect neuronal migration and formation of functional synapses. In adult brain they provide trophic support for neurons – they produce glycogen and transport lactate to neurons. They also respond to the neuronal excitation and regulate cerebral blood flow. Moreover, astrocytes play a key role in brain damage and glial scar formation (reviewed in Sofroniew and Vinters, 2010).

All types of astrocytes have one specificity in common: they create gap junctions and thus are connected into a complicated network, which is termed syncitium (Anders *et al.*, 2014; Le *et al.*, 2014). Astrocyte gap junctions are formed by connexin 43 (Cx43) and connexin 30 (Cx30) proteins, which assemble hexameric hemichannels in membranes. Two hemichannels build a gap junction and connect the cytosols of two astrocytes (Unger *et al.*, 1999). This connection allows astrocytes to carry out specialized functions, which are linked to their main role in an adult brain – maintenance of homeostasis. As was mentioned above, astrocytes create gap junctions also with other cell types, such as oligodendrocytes, and thus form one extensive panglial network through the whole brain (Liu *et al.*, 2002; Magnotti, Goodenough and Paul, 2011; Tress *et al.*, 2012).

Astrocytes maintain ionic and neurotransmitter homeostasis in CNS, especially homeostasis of glutamate. Glutamate is the main excitatory neurotransmitter in the brain,

with a wide range of functions, and its extracellular levels rise only in a response to neuronal activation. Glutamate interacts with a set of membrane receptors, that are both – ionic channels and G-protein coupled receptors. Long-term exposure to glutamate causes disruption of membrane potential in neurons and leads to their damage and cellular death (Choi, 1988). Astrocytic processes, which envelope synapses, express glutamate transporters – such as excitatory amino acid transporters (EAATs) - in abundance, and thus are able to remove glutamate rapidly from synapses and stop the signal transmission (Armbruster, Hanson and Dulla, 2016).

3.4.2 Cerebral blood flow regulation

One of the essential astrocytic functions in CNS is K^+ buffering. In the brain, K^+ is released from neurons following their increased activity, namely generation of action potentials. Astrocytes transport K^+ from extracellular space via specific channels into intracellular space and through gap junctions to the other parts of brain parenchyma, where the concentration of K^+ is low. Thanks to this redistribution an increased activity in any part of the brain does not lead to a disruption of brain homeostasis and to neuronal damage (Witthoft, Filosa and Karniadakis, 2013). K^+ is also released from astrocytic endfeet on the glia-vascular surface and influence the permeability of BBB and cerebral blood flow in connection to increased neuronal activity. The elevated concentration of K^+ causes hyperpolarization, which leads to vasodilatation of smooth muscles of arterial walls. The increased arterial diameter allows local hyperemia in the regions of the brain, which are active at the time, and thus better oxygen and glucose supply (Knot, Zimmermann and Nelson, 1996).

However, the functional hyperemia is not mediated only by K^+ ions. It strongly depends on astrocytic activation by local release of neurotransmitters, such as glutamate (Zonta *et al.*, 2003). The vasodilatory effect was noticed also in connection with arachidonic acid metabolites or astrocytic calcium signaling (Takano *et al.*, 2006). The intracellular concentration of calcium $[Ca^{2+}]_i$ in astrocytes is elevated in response to neuronal stimulation as a result of removal neurotransmitters from synapses, and $[Ca^{2+}]_i$ has an oscillating character. These oscillations can change into so-called calcium waves, which propagate through the astrocytic network (Cornell-Bell *et al.*, 1990). The increased $[Ca^{2+}]_i$ in astrocytes means an increased $[Ca^{2+}]_i$ in endfeet of the activated cells, which leads to its release via specific channels. These calcium signals correlate with enlarged arterial diameter

(Zonta *et al.*, 2003). The vasoactive effect of Ca^{2+} is not limited only to vasodilatation. It was demonstrated, that Ca^{2+} can cause also vasoconstriction (Mulligan and MacVicar, 2004). The resulting effect of calcium signaling on the brain arterioles seems to depend on the size of calcium wave and activation of signaling pathways with opposing roles in vascular endothelium (Mulligan and MacVicar, 2004).

3.4.3 Astrocyte swelling

Astrocytic endfeet at both the glia limitans and surrounding parenchymal blood vessels have been well documented to play a role in astrocytic volume changes via movement of osmolytes and water. Molecules also move through the panglial syncytium through contacts with both oligodendrocytes and with neighboring astrocytes. Uptake of osmolytes at synapses is also involved in alterations in astrocytic volume.

Astrocytic swelling is a complex process, which includes activation of a large number of membrane channels and transporters. These mediate influx of osmotically active solutes, including K^+, Na^+ or Cl^-. The ions can move through plasmatic membrane via channels, such as $Na^+/K^+/Cl^-$-cotransporter type 1 (NKCC1), TRPV4, inwardly rectifying potassium channels type 4.1 (Kir4.1), Na^+/K^+-ATPase or sulfonylurea receptor 1 (SUR1) associated with transient receptor potential melastatin 4 (TRPM4; Fig. 3). Ions then move through the panglial syncytium via connexin hemichannels. Osmotic gradients are also increased by uptake of glutamate from active synapses. Water follows these solutes via AQP4 water channels as well as through connexins and the cells swell. Individual astrocytes differ in their ability take up water and ions, because of a variability in expression of above mentioned membrane proteins. The astrocyte swelling is followed by RVD. In this process TRPV4, NKCC1 and anion channels such as volume regulated anion channels (VRAC/LRRC8), chloride channels type 2 (ClC-2) are supposedly involved. They remove ions from astrocyte cytoplasm. It causes water efflux from the cells and results in astrocytic volume decrease (reviewed in Lafrenaye and Simard, 2019).

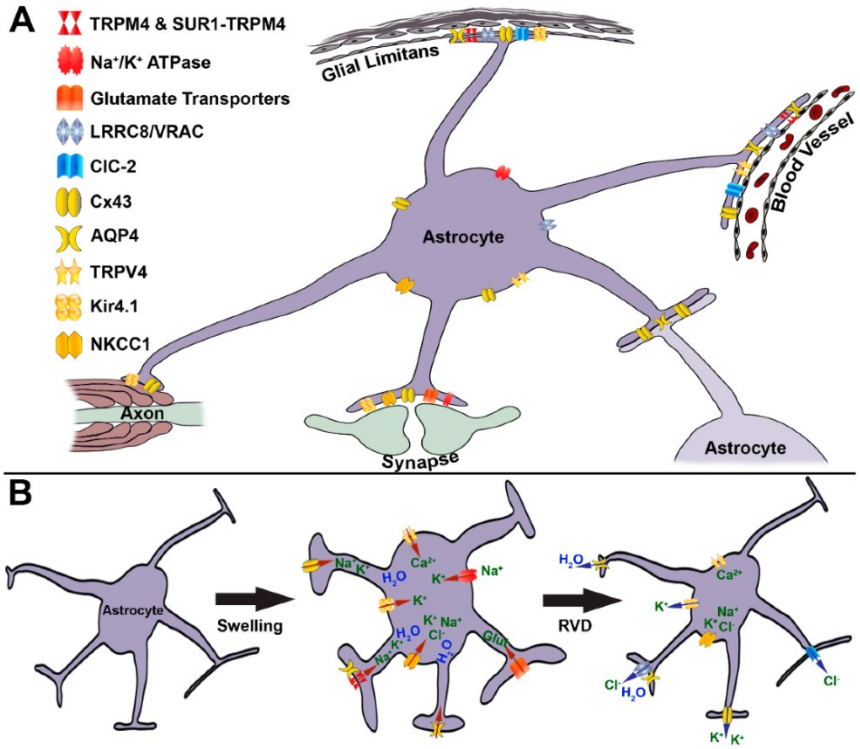

Figure 3: Astrocyte swelling and volume regulation involve multiple complex processes. (A) Illustration depicting the major sites associated with movement of osmotically active molecules into and out of astrocytes influencing astrocyte swelling. The potential localization of channels reported to regulate astrocyte swelling and/or volume decrease are also depicted; however, exact subcellular localization for many of these channels remains to be determined. (B) Summary of channels mediating astrocyte swelling (red channels) or regulated volume decrease (RVD; blue channels). Yellow channels are involved in both swelling and RVD. During astrocyte swelling, the channels colored red are involved in mediating the influx of ions and osmotically active molecules (red arrows). Swelling involves K^+ ions moving into the cell via Cx43 gap junctions and hemichannels, Kir4.1 and Na^+/K^+-ATPase. The NKCC1 and SUR1-TRPM4 channels allow the influx of multiple ions, including K+, Na^+ and Cl^-. Glutamate movement into astrocytes through transporters and Ca^{2+} influx through TRPV4 channels also increases the osmotic gradient leading to water movement into swelling astrocytes through AQP4 channels. Following swelling, the channels colored blue are involved in reducing astrocytic volume and expelling osmolytes (blue arrows). Upon RVD, K^+ moves out of individual astrocytes via Cx43, and Kir4.1 channels. Both ClC-2 and LRRC8/VRAC channels remove Cl^- from astrocytes resulting in water movement out of astrocytes through AQP4 channels. The TRPV4 and NKCC1 channels also might play roles in mediating astrocyte volume decrease, however, the mechanisms by which this happens are not yet understood. It is important to note that astrocyte swelling and RVD are complex processes with multiple players that may or may not act together in any given situation and/or following any particular pathological event and that our knowledge regarding many of these mechanisms is still limited, therefore parts of this figure are speculative. Taken from (Lafrenaye and Simard, 2019).

3.4.4 Reactive astrocytosis

Astrocytes are known to play an important role in brain pathologies and injuries. They are able to undergo a dramatic change and transformation called ‚reactive astrocytosis'. It is a state characterized by complex changes in gene expression, leading to changes in morphology. It is still discussed, whether reactive astrocytes are beneficial or harmful for the injured brain. They were proven to have both protective as well as damaging role. Reactive astrocytes protect tissue after an injury by building a barrier (glial scar) around the site of damaged tissue. Astrocytes are essential for BBB repair and recovery and their deletion of causes wide spread tissue disruption and degeneration (Faulkner *et al.*, 2004). On the contrary, reactive astrocytes inhibit axonal reparation and sprouting (spontaneous growth of neurons in response to injury) (Brambilla *et al.*, 2009) and modify the extracellular matrix causing a glial scar formation (Zamanian *et al.*, 2012). Astrocytes in healthy brain induce synapse formation, while in reactive astrocytes such ability is reduced. They do induce synapse formation, but fewer and those are weaker, compared to the healthy brain (Liddelow *et al.*, 2017).

Reactive astrocytosis is characterized by molecular changes. All reactive astrocytes show increased GFAP and vimentin (intermediate filament protein) immunoreactivity that persists for at least a week after the injury (Zamanian *et al.*, 2012), and increased level of AQP4 (Saadoun *et al.*, 2005). Their final transcriptome depends on the nature of the injury or pathology. Every astrocyte responds to the injury a little bit differently and most of the changes are transient. They are also able to divide, but this ability is limited and is delayed to the primary insult (Zamanian *et al.*, 2012). The molecular changes also suggest that reactive astrocytes posses the ability of phagocytosis, helping to decrease the amount of cellular waste accumulated due to brain injury (Morizawa *et al.*, 2017).

4 Aquaporin 4

Aquaporin 4 is a member of the aquaporin protein family, which was described by Peter Agre and his colleagues in 1990s. His laboratory identified an integral membrane protein in red blood cells, which they named CHIP28. This protein was selective for water

and was reversibly inhibited by mercuric chloride (Preston *et al.*, 1992). Later other water channels were identified not only in vertebrae, but also in plants and other groups of organisms, and today a whole family of aquaporins is known. This family consists of two main groups of channels: aquaporins (which are specifically permeable for water only) and aquaglyceroporins (permeable for water and small nonpolar solutes, such as glycerin) (Agre et al., 2002).

4.1 Structure and localization

Aquaporins are small channels with six transmembrane helixes and two semi-helixes, usually functioning as tetramers. Each type of aquaporin has a specific tissue expression pattern (Agre, 2006; Papadopoulos and Verkman, 2013). AQP4 is one of three aquaporins found in the brain, but the only one which was described in mice on astrocyte membranes and on a subpopulation of ependymal cells (Nielsen *et al.*, 1997). AQP4 is expressed in several isoforms: M1, M23, Mz, AQP4e. The major isoforms (M1 and M23) vary because of different translation initiation (more than one methionine codon is part of the genetical sequence of 5‘ untranslated region). These polypeptides of ~32 and ~34 kDa in length, differ in 22 amino acids at the N-terminus (Neely *et al.*, 1999; Furman *et al.*, 2003; De Bellis *et al.*, 2017; Lisjak *et al.*, 2017) – Fig. 4. These different isoforms indicate functional heterogeneity or different localization of each polypeptide. AQP4 assembles into homo- and heterotetramers. The tetramerization requires intracellular part of the polypeptide called D-loop. These loops of each subunit interact and stabilize the whole tetrameric structure (Kitchen *et al.*, 2016). Different tetramers have the same water permeability, specified by a highly conserved amino acid motif of asparagine-proline-alanine, but can vary in regulatory mechanisms (different phosphorylation sites) and in their localization within the brain (Neely *et al.*, 1999; Agre *et al.*, 2002). It was demonstrated that tetramerization is not required for AQP4 trafficing into the plasma membrane, however, the non-tetrameric forms are not able to respond to local osmolarity changes (Kitchen *et al.*, 2016). The different pool of each isoform also indicates that cells are able to regulate their expression as a follow up to specific conditions and homeostatic needs (Nicchia *et al.*, 2010; De Bellis *et al.*, 2017).

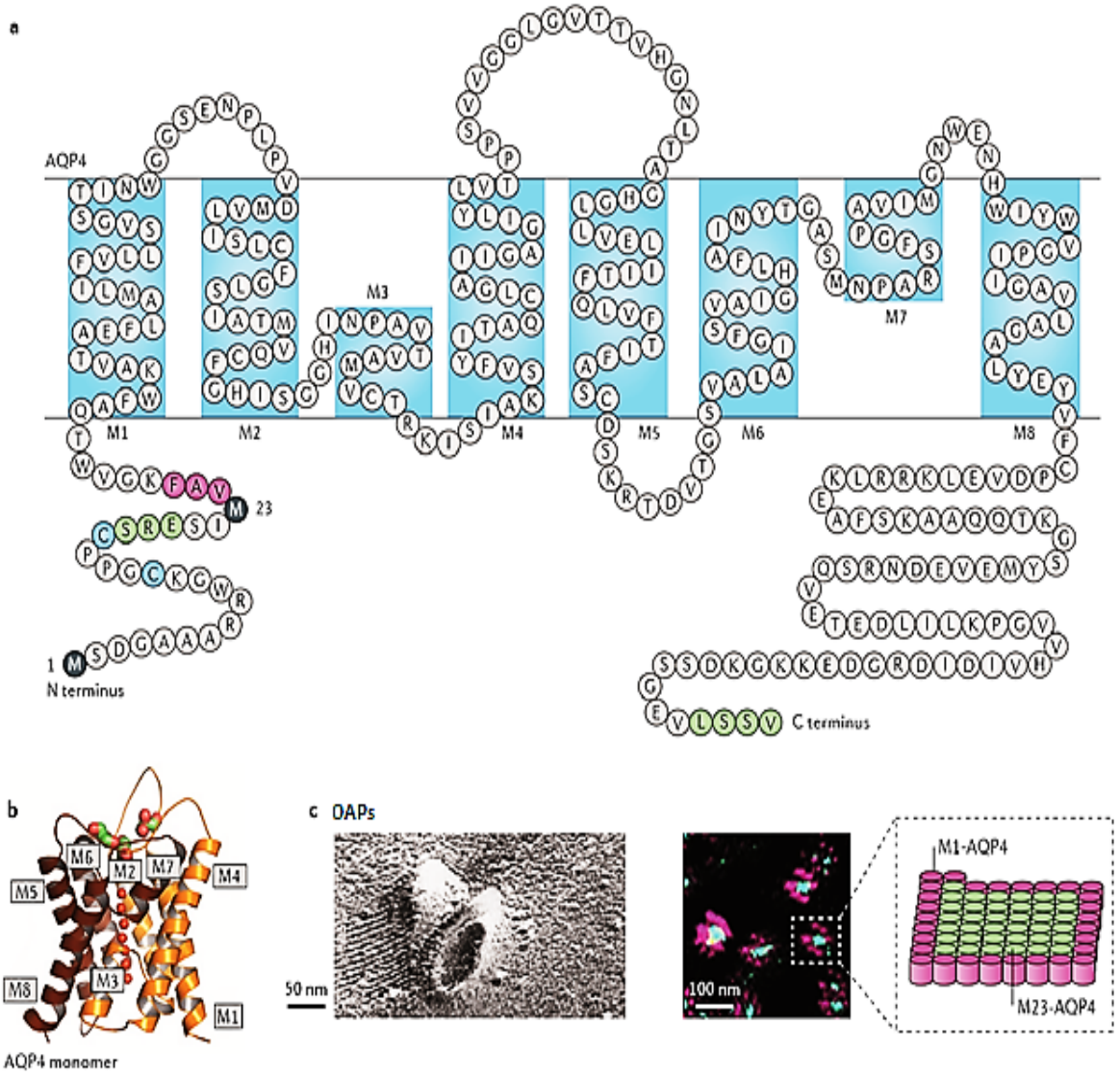

Figure 4: Sequence and structural features of AQP4. a) The primary amino acid sequence and membrane topology of AQP4. AQP4 has six transmembrane helixes and two semi-helixes, which are labeled M1 – M8. Two translation initiation sites on N terminus — Met1 and Met23 (black) — correspond to the two main AQP4 isoforms, M1 and M23. AQP4 tetramers can form orthogonal arrays of patricles (OAPs) through intermolecular N-terminal associations between M23 isoforms involving the residues highlighted in purple. The residues in green prevent N-terminal associations between M1 AQP4 molecules. Cysteine residues (in blue) are sites of palmitoylation, and are involved in regulating OAP assembly. b) X-ray crystal structure of human AQP4 shows the eight membrane helixes. c) Freeze-fracture electron micrograph of M23-AQP4-OAPs (left panel). The middle panel shows a super-resolution micrograph of cells co-expressing a green fluorescent variant of M23-AQP4 and a red fluorescent variant of M1-AQP4. From such micrographs, it has been determined that OAPs have a M23-AQP4-enriched core, with M1-AQP4 being found in the periphery of these structures. Taken from: Papadopoulos and Verkman, 2013.

The expression of AQP4 on astrocyte membranes is highly polarized. Using immunolabeling techniques, AQP4 was found to be predominantly expressed on endfeet, i.e. the processes in direct contact with blood vessels, and in *glia limitans* (Nielsen *et al.*, 1997; Neely *et al.*, 1999). On this membranes, the expression is so strong, that AQP4 tetramers can assemble into supramolecular structures, called orthogonal arrays of particles (OAPs) (Rash et al., 1998; Neely et al., 1999; Sorbo et al., 2008). These are formed from ~ 6nm intermembrane particles, which can be separated or create clusters (OAPs). In one OAP up to 100 tetramers can be found (Furman *et al.*, 2003; Smith and Verkman, 2015). The size of each OAP is determined by the ratio between AQP4 isoforms (Sorbo *et al.*, 2008; Nicchia *et al.*, 2010; De Bellis *et al.*, 2017). When expressed alone, the M1 and Mz isoforms create isolated particles, contrary to M23, which forms large OAPs – Fig. 4. But all isoforms expressed together form average size OAPs, with the size dependent on the isoforms ratio (Sorbo *et al.*, 2008; Nicchia *et al.*, 2010; Smith and Verkman, 2015). The supramolecular assembly is also a determinant of subcellular localization of the AQP4 tetramers. The large OAPs seems to be preferentially expressed on astrocyte endfeet, while the separate tetramers and smaller clusters localize on the other parts of astrocytes and on the cells, which are not in the direct contact with capillaries (Smith and Verkman, 2015). The polarization of AQP4 expression and its localization on blood-brain interface is dependent on α-syntrophin, a protein, which anchors OAPs in the membranes on the astrocyte-capillary interface (Neely *et al.*, 2001). In animals lacking α-syntrophin the total level of AQP4 expression is unaltered, but its molecules are not so specifically localized as a part of BBB (Neely *et al.*, 2001).

Besides α-syntrophin, AQP4 is suspected of creating supramolecular complexes with other channels. One of them is Cx43. Cx43 is the main protein creating gap junctions in the brain and thus allows water and ions to redistribute within the astrocytic syncytium. However, its functional connection with AQP4 remains unclear, because in literature contradictory opinions can be found. In cultured neonatal mouse astrocytes knocking down the AQP4 gene caused strong down-regulation of Cx43, but in human cortical cultured astrocytes, the protein levels were not altered (Nicchia et al., 2005). On the contrary, the number of Cx43 - together with Cx30 - was increased in adult brain tissue of AQP4-deficient mice (Katoozi et al., 2017), showing probably some kind of developmental regulation. Furthermore, AQP4 was described to create a complex with TRPV4 in cultured cells (Benfenati et al., 2011) and in Muller glia in the retina (Jo et al., 2015), as well as a complex with Kir4.1 (Jo et al., 2015). The latest, however, does not include any functional coupling

between AQP4 and Kir4.1. It seems to be the matter only of high protein expression within the BBB (or blood-retina barrier) (Zhang and Verkman, 2008), but the results remain unclear.

4.2 AQP4 in brain pathologies

AQP4 is studied intensively, because of its crucial role in many brain pathologies, such as brain edema and ischemia, non-specific complications accompanying other diseases and injuries, such as stroke, traumatic brain injury, tumors or liver failure (Klatzo, 1987; Unterberg et al., 2004). Interestingly, AQP4 seems to play opposite roles in both types of brain edema. Its localization on astrocyte endfeet makes AQP4 an essential part of BBB and thus an influx route for water in pathological conditions of the vasogenic edema (Camassa et al., 2015), which is caused by increased permeability of brain capillaries and thus by BBB disruption. Serum proteins enter the brain parenchyma without limitations and cause a massive water influx, even through undamaged parts of brain capillaries. This results in expansion of extracellular space and compression of cellular compartments of the brain tissue. The process of water accumulation also causes an increase in intracranial pressure (Fishman, 1975; Klatzo, 1987). In a healthy brain, the extracellular fluid is eliminated through *glia limitans* (and through AQP4 channels) and into subarachnoid space, as well as into capillaries and cerebrospinal fluid (Fenske and Prioleau, 1978; Tait et al., 2008). In the case of vasogenic edema, the AQP4-deficient mice have shown a significant increase in brain water content. In these mice, physiological water elimination via AQP4-rich *glia limitans* does not occur and water accumulates within the brain parenchyma (Manley et al., 2004; Tang et al., 2010). On the contrary, the outcome of cytotoxic edema in AQP4-deficient mice is better, compared to the wild-type animals. The role of AQP4 in pathological cytotoxic swelling was demonstrated in several studies using AQP4-deficient mice, showing improved outcomes in models of ischemic brain injury, such as MCAO (Yao et al., 2015; Hirt et al., 2016). These mice have significantly lower mortality, compared to the wild-type mice, as well as significantly smaller lesion volume (Manley et al., 2000; Akdemir et al., 2014; Katada et al., 2014; Yao et al., 2015; Hirt et al., 2016). Stroke or traumatic brain injury usually leads to reactive astrocytosis. This process is influenced by many factors, and one of them is the presence/absence of AQP4. Reactive astrocytes are able to migrate to the specific area of the damage and this ability, and the glial scar formation itself is disrupted in AQP4-deficient mice (Saadoun *et al.*, 2005).

AQP4, however, plays an important role also in other brain pathological states, such as neuromyelitis optica (NMO). It is an autoimmune demyelinating disease affecting predominantly optic nerves and spinal cord. In serum of patients with NMO, a specific immunoglobulin type G (IgG) was found. This antibody binds to capillaries and to the subpial surface of the brain, where AQP4 is strongly expressed (Lennon *et al.*, 2005). Recent extensive research indicates, that AQP4 has its role even in processes leading to depression (Kong *et al.*, 2014) or in the long-term memory (Fan *et al.*, 2013).

4.3 Regulatory volume decrease

AQP4 and other proteins in close coupling with AQP4 such as TRPV4 or Kir4.1, are considered to be the key players in the process of astrocytic regulatory volume decrease (RVD), which occurs during in cytotoxic edema and comprises an efflux of osmolytes, such as taurine, aspartate and Cl^- (Benfenati et al., 2011; Mola et al., 2017). Cytotoxic edema is caused by homeostatic imbalance and leads to water accumulation inside the cells (Baethmann, 1978). Astrocytes are able to react to the pathological hypoosmotic conditions by stimulating AQP4 expression and thus by forming new OAPs and by redistributing AQP4 proteins within the cells, as was described on astrocyte cultures (Lisjak et al., 2017). That affects the dynamics of water transport in brain parenchyma and leads to the RVD. Astrocytic response to the extracellular hypotonicity involves an increase in $[Ca2^+]_i$ (Benfenati et al., 2011), which is, however, just a consequence of increased permeability of the plasma membrane and it does not function as an intracellular signal (Morales-Mulia *et al.*, 1998). The process of RVD might involve also other protein channels, such as Kir4.1 or TRPV4.

5 Transient Receptor Potential Vanilloid 4 channels

TRPV4 is a member of transient receptor potential (TRP) channels family, a large class of proteins, which is widely distributed in mammalian tissues and have a wide range of functions. TRP channels are permeable for monovalent cations and for Ca^{2+}, which makes them an important component of Ca^{2+} signaling pathways (reviewed in Clapham, Runnels and Strübing, 2001).

TRPV4 is a tetrameric channel with structure homologous to other members of the TRPV family (Shigematsu *et al.*, 2010). It has 5 splicing variant with alternations in the N-terminal region (Arniges *et al.*, 2006) and individual subunits can assemble into homo- or heterotetramers. The assembling can influence TRPV4 localization or modify the functioning of these channels. The similar effect has an alteration in the C-terminal domain (Arniges *et al.*, 2006; Becker *et al.*, 2008; Deng *et al.*, 2018). Through N-terminus the TRPV4 channels are able to interact with other effector proteins, that modify their activity and the activity of downstream signaling cascades (Garcia-Elias *et al.*, 2013). One of such proteins is phosphatidylinositol-4,5-bisphosphate (PIP_2). Its role in TRPV4 activation/deactivation, however, remains unclear. Harraz and colleagues suggested, that in capillary endothelium in brain PIP2 inhibits TRPV4 channels and this inhibition can be reversed by reducing PIP2 concentration in endothelial cells (Harraz *et al.*, 2018). On the contrary, Garcia-Elias et al., 2013 found, that PIP2 binds to TRPV4 through a binding site in N-terminal domain and such interaction rearranges intracellular domains of TRPV4 leading to its activation.

5.1 TRPV4 functions

TRPV4 channel is a polymodal receptor and is able to respond to various stimuli, such as cell swelling, acidity changes or mechanical stress (reviewed in Kanju and Liedtke, 2016). As a member of the TRP family, TRPV4 channel is temperature sensitive, with its optimum between 27 – 37°C (Güler *et al.*, 2002; Watanabe *et al.*, 2002). It has a wide range of functions across various tissues. In the brain, it was reported to stimulate OPCs proliferation via its activation. Thus TRPV4 channels may be involved in brain development and plasticity (Ohashi *et al.*, 2018). Besides OPCs, TRPV4 is expressed also on other cell types in CNS and through most of the mammalian tissues.

TRPV4 channels are expressed on neuronal membranes, where they play an important role as osmosensors and thus are involved in neuronal volume regulation. TRPV4 activation leads to Ca^{2+} influx into the neurons and this Ca^{2+} entry acts as an activating signal for other ion channels. TRPV4 channels were shown to functionally couple with Ca^{2+}-activated K^+ channels (K_{Ca}) and their activity causes an influx of K^+ into the neurons resulting in their hyperpolarization (Feetham *et al.*, 2015).

TRPV4 channels are expressed also on astrocytic membranes, however, its expression is restricted to about 20 – 30 % of astrocytes within the brain (Shibasaki *et al.*, 2014).

TRPV4-positive astrocytes are suspected to play a role in the synchronization of neuronal excitability via a release of regulating proteins (so-called gliotransmitters), such as adenosine triphosphate or glutamate (Shibasaki *et al.*, 2014). These channels also influence neurovascular coupling (NVC). This term describes a close relationship between neuronal activity and vascular dilatation/constriction, with astrocytes as an intermediate. This process is partially mediated by Ca^{2+} (and thus by TRPV4 channels), which is released from astrocytic endfeet and causes vasoconstriction (Mulligan and MacVicar, 2004). NVC is also regulated via a release of K^+ and nitric oxide (Kenny, Plank and David, 2018).

5.2 TRPV4 in brain pathologies

TRPV4 channels play their role in brain pathologies and they even have their role in channelopathies, which are hereditary and affect TRPV4 functions. Most of them do not affect CNS, but are of motoric nature, affecting lungs or PNS (reviewed in Nilius and Voets, 2013). In CNS, this channel is also involved in demyelinating diseases (Liu *et al.*, 2018).

TRPV4 channels provide a bidirectional pathway for Ca^{2+} and their activation increases Ca^{2+} signaling in astrocytes as well as cell membrane depolarization (Lipski *et al.*, 2006; Dunn *et al.*, 2013; Rakers, Schmid and Petzold, 2017). Ca^{2+} signaling is increased in ischemic conditions, because TRPV4 channels are known to respond to various stimuli occurring during ischemic events, such as membrane stretch and changes of pH. The pathological state such as global cerebral ischemia also leads to upregulation of TRPV4 expression on astrocytes (Butenko *et al.*, 2012). This modulates functioning of signaling pathways, that regulate cell death and survival, such as mitogen-activated protein kinase (MAP-kinase) pathway. During ischemia, TRPV4 channels were shown to amplify tissue damage and BBB disruption via over-activation of apoptotic pathways (Pinghui Jie *et al.*, 2015). Using TRPV4 antagonist reduced brain-infarction area after MCAO of about 30 % in mice (P. Jie *et al.*, 2015).

TRPV4 channels are suspected to function as a complex with AQP4 channels (Fig. 5). AQP4 and TRPV4 are trafficked independently to the membrane, and also their activation and functioning can be autonomous (Jo *et al.*, 2015). But in cultured astrocytes and in Muller glia in retina, these channels were shown to colocalize (Benfenati *et al.*, 2011; Jo *et al.*, 2015). Because of this colocalization, both channels are supposed to be key players in the process of astrocytic RVD. This osmoregulating complex can be the link between cell water

permeability and Ca^{2+} homeostasis, that seems to be the trigger for a cellular response, leading to RVD or even to apoptosis (Iuso and Križaj, 2016). It is even hypothesized that RVD cannot occur without both components present on the membrane (Benfenati *et al.*, 2011). Taken together, this indicates, that TRPV4 is an important player in astrocytic Ca^{2+} signaling events during ischemia (Rakers, Schmid and Petzold, 2017).

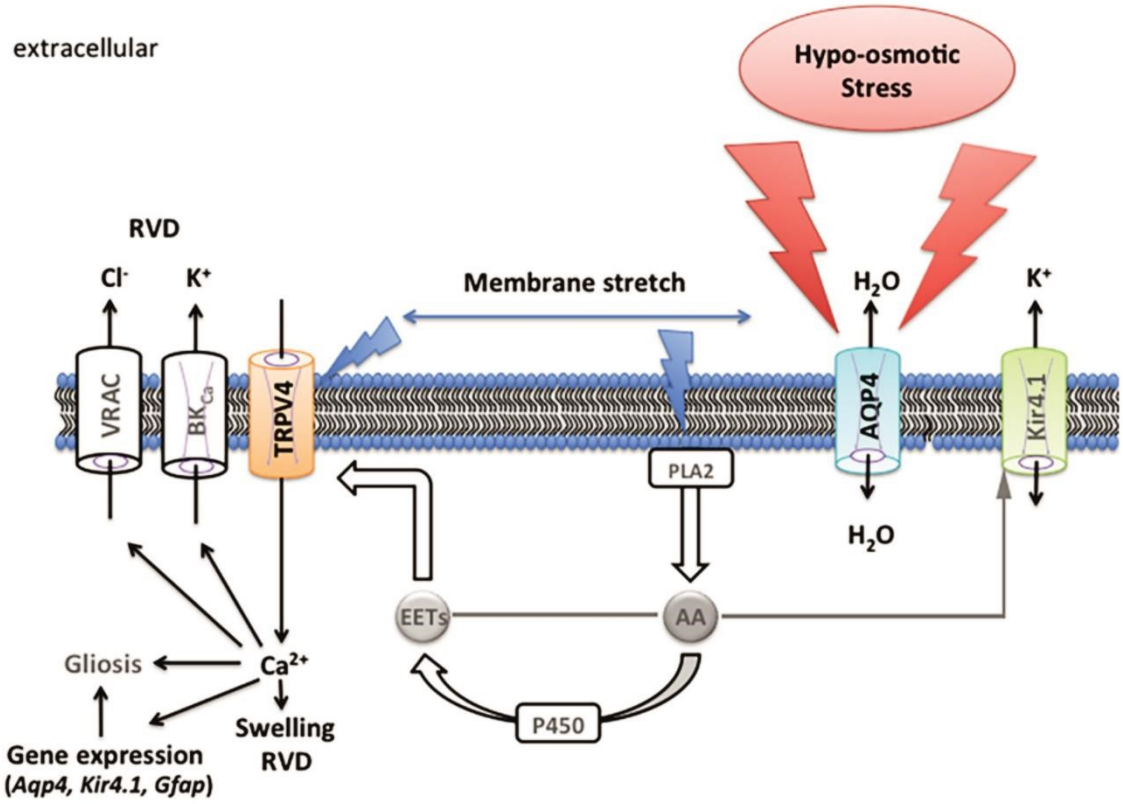

Figure 5: Proposed schema of TRPV4 – AQP4 interactions in the Müller cell endfoot. Hypotonic stress stimulates fluxes of water after the osmotic gradient. The resulting increase in cell volume stretches the plasma membrane, activating TRPV4 and a Ca^{2+} and stretch-sensitive phospholipase A2 (PLA2). The product, arachidonic acid (AA), is a precursor for the cytochrome P450-mediated synthesis of eicosanoid metabolites (EETs) that serve as final activators of TRPV4 channels but may also suppress Kir4.1 The expression of Kir4.1 and reactive gliosis are modulated by hypotonic stimulation-induced influx of Ca^{2+}. It remains to be determined whether stretch activates PLA2 simultaneously with TRPV4 or whether its activation, which is Ca^{2+}-dependent, amplifies the initial TRPV4 signal (blue arrows). Ca^{2+} induces both cell swelling (short term) and RVD (long term) and may be required for Ca^{2+} dependent gene expression (Aqp4, Kir4.1, Trpv4, Gfap). High levels of Ca^{2+} may also stimulate the activity of big potassium (BK) and VRAC channels and facilitate RVD. Taken from: Jo *et al.*, 2015.

6 Methods

6.1 Animals

Experiments were performed on GFAP/EGFP transgenic mice (line designation TgN(GFAP-EGFP), FVB background), in which the expression of enhanced green fluorescent protein (EGFP) is controlled by the human GFAP promoter (Nolte *et al.*, 2001). These animals were either crossed with the TRPV4-deficient strain (on C57BL/6N background) with excised exon 12 encoding transmembrane pore domains 5 and 6 (Liedtke and Friedman, 2003) or with AQP4-deficient mice. Those were generated as previously described Ikeshima-kataoka *et al.*, 2013 and frozen embryos were obtained from Riken BRC (acc. no. CDB0758K-1; http://www.cdb.riken.jp/arg/mutant%20mice%20list.html; genetic background B6 mixed with Balb/c) and derived by a licenced carrier to the Czech Republic, were breeding lines were established through embryo transfer. Homozygous TRPV4- and AQP4-deficient lines were established together with homozygous TRPV4- and AQP4-positive lines, used as controls.

All procedures involving the use of laboratory animals were performed in accordance with the European Communities Council Directive 24 November 1986 (86/609/EEC) and animal care guidelines approved by the Institute of Experimental Medicine, Czech Academy of Sciences (Animal Care Committee on April 7, 2011; approval number 018/2011). All efforts were made to minimize both the suffering and the number of animals used.

6.2 Acute brain slices preparation

Astrocytic volume was quantified *in situ* in four groups of mice (both male and female) of the age of 90 ± 10 days. Animals were anaesthetised using intraperitoneal injection of pentobarbital (100 mg/kg) and than transcardially perfused with cold (4 ± 1 °C) isolation solution (Tab. 1). Perfused animals were decapitated and the brains were quickly removed. Acute coronal slices were prepared from each brain (300 μm thick) on a vibrating microtome (HM 650 V, Thermo Scientific Microm, Walldorf, Germany). The slices were kept in preheated (34°C) isolation solution for 30 minutes and than for another 30 minutes at room temperature in arteficial cerebrospinal fluid (aCSF; Tab. 1). Before microscopic scanning, every slice was incubated for 10 minutes in preheated aCSF (34°C), and kept

heated also during the measurement (32 ± 1 °C). Both isolation solution and aCSF were bubbled with 95% O_2 / 5% CO_2, pH 7.4, osmolality was measured using a vapor presure osmometer (Vapro 5520, Wescor, Logan, UT).

Table 1: Composition of the experimental solutions. All the concentrations are in mM.

Contents	Isolation solution	aCSF	Hypotonic solution	OGD
NaCl	-	122	67	122
NMDG-Cl	110	-	-	-
KCl	3	3	3	3
$NaHCO_3$	23	28	28	28
Na_2HPO_4	1.25	1.25	1.25	1.25
$CaCl_2$	0.5	1.5	1.5	1.5
$MgCl_2$	7	1.3	1.3	1.3
Glucose	20	10	10	-
Osmolarity [mOsm/kg]	~300	~300	~200	~300
Saturated with	95% O_2 5% CO_2	95% O_2 5% CO_2	95% O_2 5% CO_2	5% O_2 5% CO_2 90% N_2

6.3 Three-dimensional multiphoton morphometry *in situ*

Fluorescent images were acquired from acute brain slices using multiphoton laser scanning microscope FV1200MPE (Olympus) with 60x LUMPLFLN water objective. Fluorescence of EGFP was excited by 950 nm and the signal was detected using appropriate emission filters. Whole cells (cortical layer 2 – 5 astrocytes) were imaged as a set of focal images (Z-stack) with a constant spacing/step size of 0.5 µm. Approximately 150 – 200 focal images were acquired for every cell. Five Z-stacks were acquired before the experiment, for correction of scanning photobleaching. Then two sets of images were acquired 10 and 20

minutes after application of hypotonic solution/OGD solution (Tab. 1) and another two sets of images after repeated application of aCSF (10 and 20 minutes) – (Awadová *et al.*, 2018; Pivonkova *et al.*, 2018; Fig. 6).

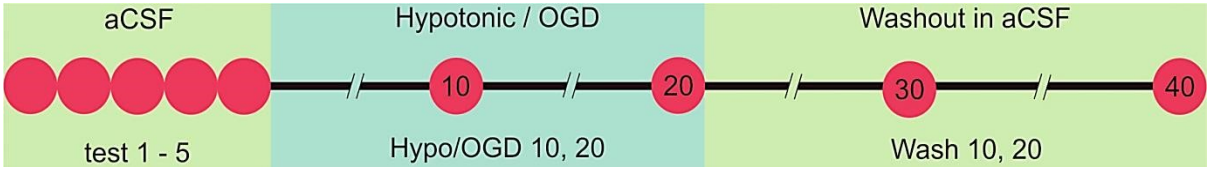

Figure 6: Schematic representation of our experimental protocol. Red circles represent each image acquisition. At the beginning of every experiment we acquired 5 sets of images for photobleaching correction (left green part, test 1 – 5). Afterwards the slices were placed in the hypotonic or OGD solution and the Z-stacks were acquired every 10 minutes (Hypo/OGD 10, 20). Then the aCSF application was repeated in washout phase and Z-stacks were acquired after 10 and 20 min of the application (Wash 10, 20).

6.4 Quantification of astrocytic volume changes

Quantification of cellular volume changes was performed using several methods. Those were described in separate methodological publication (Awadová *et al.*, 2018). Firstly we used an custom-made CellAnalyst program (Chvátal, Anděrová and Kirchhoff, 2007). The cell boundary was determined in each x-y frame using an intensity-based edge-detecting algorithm, and the area of the image surrounded by the edge was calculated for each layer. From these data, cell volume was obtained by integrating the values of all images in a stack (Awadová *et al.*, 2018). Second method we used was fluorescence intensity-based cell volume quantification in the cell soma (Awadová *et al.*, 2018; Pivonkova *et al.*, 2018). Image processing and morphometry measurements were performed using the ImageJ/Fiji software (https://fiji.sc/). From all time courses (9 Z-stacks) for one cell average fluorescence intensity projections along the z-axis were created. For projections we used only astrocytic soma. These projections were used for creating another stack of images, where the somata were aligned. The intensity of fluorescence was measured from circular selection (~ 2µm in diameter) from the cell soma (the selection was the same through all the time courses of one cell). Since the fluorescence intensity decreases proportionately to the swelling of the cells, we counted the cellular volume as 1/fluorescence intensity.

The astrocyte volume at t = 0 min (test5) was set to 100% and the astrocytic swelling was expressed relative to this baseline as an increase in percentage.

6.5 Quantification of volume changes in astrocytic endfeet

The endfeet thickness was measured from Z-stack images, as was the astrocyte volume. From the Z-stacks average projection was created in FIJI, using 3 slices, where the endfeet appeared the thickest. In these projestions the diameter of the endfeet was measured. Data were converted to relative numbers and statistically evaluated. Again, the astrocyre endfeet at time 0 (test 5) was set to 100 % and the volume changes were expresed relative to this baseline as an increase in percentage.

6.6 Statistics

The data are shown as mean ± standard error of the mean (SEM) for n cells. Two-way ANOVA with Bonferroni's multiple comparison post-test was used to evaluate significant differences in cellular volume. Values of $p < 0.05$ (*; #) were considered significant, $p < 0.01$ (**; ##) very significatnt and $p < 0.001$ (***; ###) extremely significant.

7 Aims of the study

AQP4 and TRPV4 channels are both involved in astrocytic volume regulation *in vitro*, as described Benfenati *et al.*, 2011, Iuso and Križaj, 2016. Therefore we hypothesised that similar involvement in astrocytic volume regulation should be visible also *in situ* in acute brain slices. In the the present diploma theses, we aimed to clarify roles of AQP4 and TRPV4 channels *in situ* in single astrocytes in two different pathological stimuli – hypotonic stress and OGD. We also aim to compare our results from acute brain slices with the known data from cultured cells and to adress possible differences in astrocytic volume regulation *in vitro* and in acute brain slices (*in situ)*.

8 Results

8.1 Quantification of cell volume changes

First we compared different methods of cellular volume quantification. Since our initial measurements revealed that the astrocytic volume changes detected at 30 – 32°C are too extensive, we were not able to quantify the cell volume using 3D morphometric approach. Therefore we decided to compare several methods to select the most reliable one. The first method uses a 3D morphometric analysis of the Z-stacks of images, which leads to the direct cell volume assessment (Chvátal, Anděrová and Kirchhoff, 2007). The second method derives the volume changes from area accupied by the cells in a single two dimensional (2D) image. The last approach uses the local intensity of fluorescence, which is proportional to the concentration of the fluorophore in the whole cell and is also inversely proportional to the cell volume.

The performance of the three volumetric methods - 3D morphometry, 2D morphometry and fluorescence intensity measurements – was first checked in two adherent cell cultures with different cell-shape characteristics. On the one hand, we chose 3T3 murine fibroblasts as an example of compact, morphologically well-defined cells with a vast majority of the cell volume concentrated in the close vicinity of the cell nucleus. On the other hand, a culture of cortical astrocytes isolated from a brain of GFAP/EGFP mice was chosen. Even in the single-layer adherent culture, the astrocytes develop numerous processes, which typically

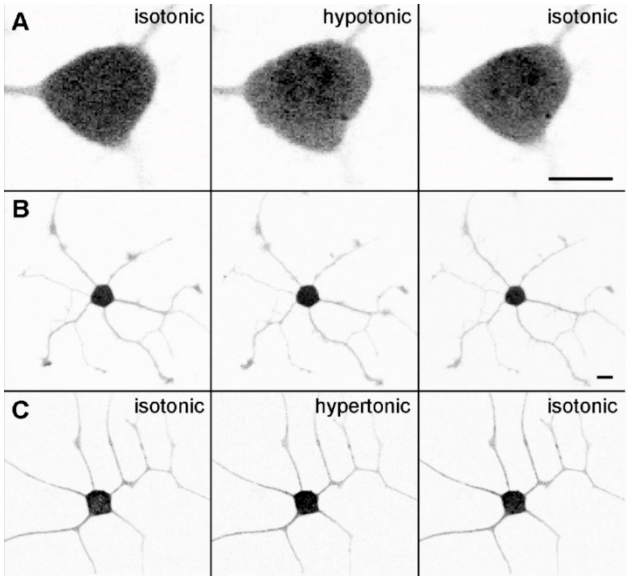

Figure 7: Cells in cultures undergoing volume changes induced by osmotic treatment. Representative lateral setion of a singlecalcein loaded murine fibroblast (A) and cortical astrocyte of GFAP/EGFP mouse in the culture (B, C) before the treatment (left), 10 min after the application of either hypotonic (205mOsm/kg; A, B) or hypertonic (405 mOsm/kg; C) solution (middle), and 5 min after the washout with isotonic solution (right) are presented. Bars: 10 µm. Taken from: Awadová *et al.*,

protrude many tens of micrometers from the globular soma, frequently branch, are not easily trackable in the culture, and markedly contribute to the cell volume (compare the different cell morphologies illustrated in Fig. 7).

Fibroblasts were preloaded with one of the accepted volume indicators, calcein-AM. Calcein-AM represents a small, plasma membrane-permeable dye that is cleaved by intracellular esterases. Membrane-impermeant fluorescent cleavage product then stays in the cytoplasm. GFAP/EGFP mouse is a transgenic mouse, the astrocytes of which are labeled by EGFP expressed under the control of the cell-type specific, human glial fibrillary acidic protein promoter (Nolte, 2001). In both cultures, the cell volume increase was induced by a standard hypotonic treatment (see Methods for detailed description). The hypotonicity-

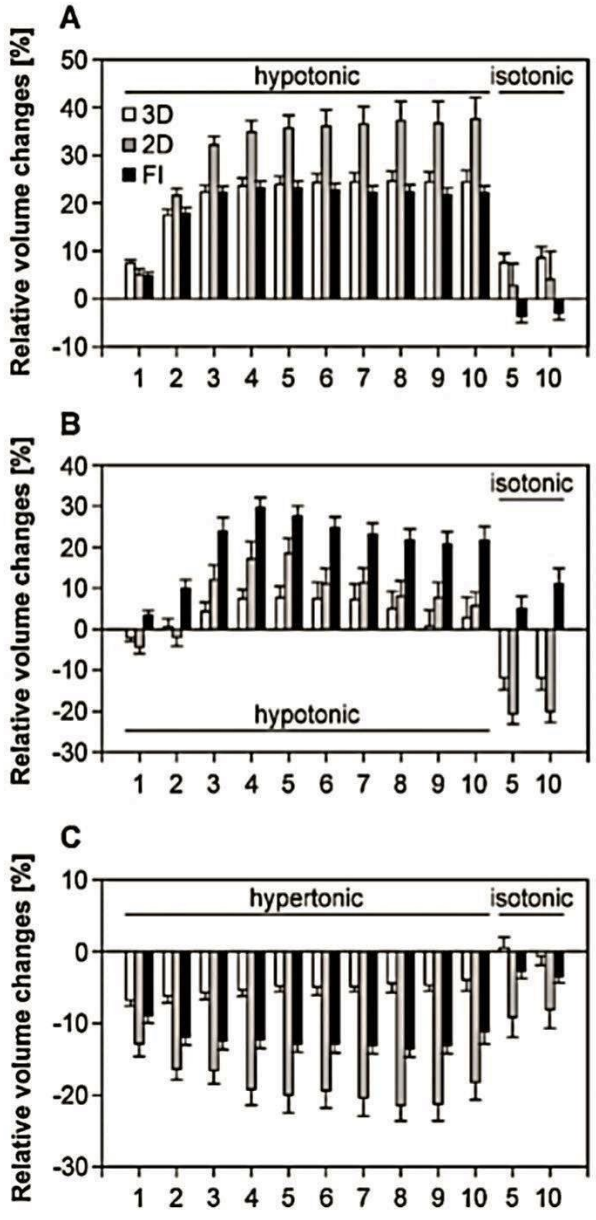

Figure 8: Quantitative analysis of cell volume changes in cell cultures. Relative cell volume in a culture of calcein-loaded murine fibroblast (A) and cortical astrocytes of GFAP/EGFP mice in the culture (B, C) as reported by 3D morphometry (3D, white bars), lateral cell size measurements (2D, gray) and fluorescence intensity measurements (FI, black) are plotted in charts. Mean values ± SEM are presented (n = 32, 28 and 17 in A, B, C respectively). Numbers along the horizontal axis indicate the time (in min) after the last exchange of the media. Taken from: Awadová *et al*., 2018.

induced swelling of individual cells was measured by the three aforementioned approaches as described in the Methods.

In both analyzed cultures, the treated cells exhibited a maximal swelling 4 min after the application of the hypotonic solution. This rapid volume increase was successfully detected by all three approaches (Fig. 8). In the fibroblast culture, 3D morphometry and fluorescence intensity methods produced identical results with a maximal volume increase by 25 ± 2% and 23 ± 2% of the initial cell volume, respectively, while the 2D morphometry approach reported somewhat higher values of the volume increase with the maximum at 38 ± 3%. After the isotonic washout, all of the three methods reported a nice restoration of the initial fibroblast volume (Fig. 8A). In the culture of cortical astrocytes, only the fluorescence intensity measurement was able to report comparable swelling amplitudes, with the maximum of 30 ± 3% (4 min after the hypotonic shift) and equilibrium at 22 ± 2% (≥8 min). Morphometric approaches detected lower swelling amplitudes with maxima of 19 ± 3% and 8 ± 2% for 2D and 3D morphometry, respectively. Both of the morphometric approaches apparently underestimated the cellular volume following the isotonic washout at the end of the experiment (Fig. 8B).

The changes in the cellular volume were quantified in a culture of cortical astrocytes from GFAP/EGFP mice by the three volumetric approaches. Again, all three approaches were capable of detecting the cell shrinkage (Fig. 8C) and again, the 3D morphometric approach revealed the smallest amplitude of the registered volume change of -7 ± 1%. The shrinkage detected by 2D morphometry and fluorescence intensity approaches were significantly ($p < 0.001$) larger, −21 ± 2% and −13 ± 2%, respectively.

Next, we compared the outputs of the three volumetric approaches in monitoring the osmotically induced volume changes of astrocytes in acute brain slices of GFAP/EGFP mice. Astrocytes in acute brain slices are cells of a highly complex architecture. Tracing their borders thus represents a serious challenge for morphometric algorithms (Bindocci et al., 2017). The application of hypo- and hypertonic treatment induced significant, but to a high extent reversible changes in the 3D morphology of these cells (Fig. 9). As expected, we observed much higher rates of astrocytic swelling in hypotonically treated brain slices, if compared to the astrocytes in the culture. After 20 min of the hypotonic treatment, 3D morphometry, 2D morphometry and fluorescence intensity measurements indicated a cell volume increase by 53 ± 7%, 105 ± 4%, and 107 ± 8%, respectively. All three approaches

also detected a significant ($p < 0.001$) decrease of the cell volume towards the original value following the re- application of the isotonic solution (Fig. 10A).

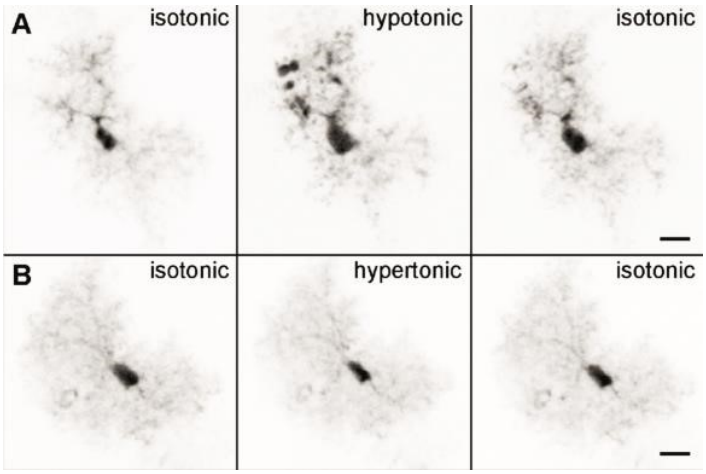

Figure 9: Osmotic treatment-induced changes of the astrocytic volume in acute brain slices. Maximum intensity projection of representative cells in acutebrain slices of GFAP/EGFP mice before the treatment (left), 20 min after the application of either hypotonic (205 mOsm/kg; A, B) or hypertonic (405 mOsm/kg; C) solution (middle), and 10 min after the washout with isotonic solution (rigDht) are presented. Bars: 10 µm. Taken from: Awadová et al., 2018.

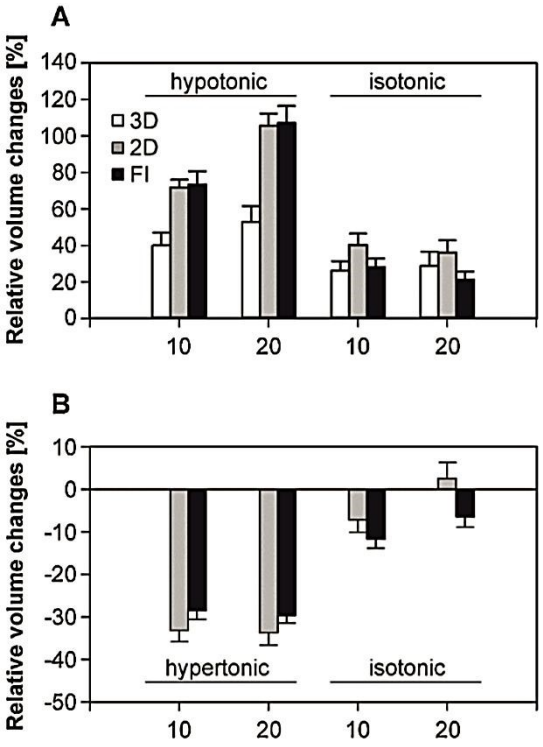

Figure 10: Quantitative analysis of cell volume changes in acute brain slices. Relative volume changes in acute brain slices of GFAP/EGFP mice induced by hypo- (A) and hypertonic treatment (B) as reported by 3D morphometry (3D, white bars), lateral cell size measurements (2D, gray) and fluorescence intensity measurements (FI, black) are reported in charts. Mean values ± SEM are presented (n = 49 and 13 in A and B, respectively). Numbers along the horizontal axis indicate the time (in min) after the last exchange of media. Taken from: Awadová et al., 2018.

The peripheral parts of the astrocytes with a terminally branching bushy network of fine processes were hard to trace (Fig. 9), which was especially true in the axial (z) direction within the 3D image stacks. A typical astrocyte cell encompassed 150–200 x-y frames on a z-stack. It has to be mentioned that, despite the use of a two-photon fluorescence excitation, the contrast of the images recorded deeper in the tissue was significantly lower when compared to the more superficial ones. The number of frames further increased upon the swelling of the brain section during the hypotonic treatment. This fact could contribute not only to a significantly ($p < 0.001$) lower amplitude of the volume changes detected by the 3D morphometry method, but also to the relatively high standard deviation of the values measured by the 3D morphometry approach in this type of specimen. As an additional control of the cell integrity during the osmotic changes applied to the acute brain section, a hypertonic solution was applied to the specimen. In this case, only 2D images of the analyzed cells were acquired. A comparison of relative cell volume changes, as revealed by 2D morphometry and fluorescence intensity, is presented in Fig. 10B. The maximum cell shrinkage detected by these approaches was −30 ± 2% and −33 ± 3%, respectively. After 20 min of isotonic washing, the cell volume was restored to the original values. We concluded that the applied osmotic changes did not have a deleterious effect on the integrity of the analyzed astrocytes.

Finally, we analyzed the cell volume changes as registered by the three approaches in astrocytes in acute brain slices of GFAP/EGFP mice during hypotonic treatment performed either at room temperature (RT, 23 °C), or at a temperature of 32 °C (HT). The samples were treated as described above. In HT, a higher amplitude of astrocytic swelling can be expected due to various reasons. Among others, plasma membrane biophysics and the activity of transport proteins integral to the plasma membrane are temperature sensitive. In agreement with our expectations, the registered increase of the cell volume was in general higher in the HT samples. After 10 min of the hypotonic treatment, all three approaches registered significantly higher astrocyte swelling in the HT samples, when compared to RT. However, in the case of the 3D morphology approach, this was the only time point to confirm that. Later on, 3D morphology approach reported comparable volume changes for both temperatures. We concluded that in contrast to 2D morphology and fluorescence intensity approaches, 3D morphometry failed to register temperature-induced increase in the astrocyte swelling in this experiment.

We compared all the results of methods listed above *in vitro* and *in situ* (Fig. 7-10) and concluded that fluorescence-based volume measurements were the most reproducible and were in fact insensitive to the cell shape complexity. The results of this study were published by Awadová *et al.*, 2018. Thanks to the high complexity of astrocytes we decided to use the fluorescence-based approach to quantify their volume in our experiments.

8.2 Volume changes of astrocytes from AQP4- and TRPV4-deficient mice

In order to examine the role of AQP4 and TRPV4 channels in astrocytic swelling we quantified cell volume of single astrocytes together with endfeet thickness *in situ* in cortex of adult mice (90 ± 10 days). In total we measured 175 cells of three different goups of animals (Control (Ctrl), AQP4-deficient ($AQP4^{-/-}$), TRPV4-deficient ($TRPV4^{-/-}$) under two different conditions (two pathological stimuli – hypotonic stress and OGD).

We performed our experiments on GFAP/EGFP mice, both males and females, because there were no differences between them in expression of both channels (Liu *et al.*, 2008). Our experimental protocol included 5 control measurements of each cell, performed in aCSF solution for correction of photobleaching of EGFP. Then the hypotonic or OGD solution was applied to the brain slices for 20 minutes. This was followed by 20-min phase of washout. The images were acquired every 10 minutes (Fig. 11). All the measurements were performed in 32 – 34°C, for TRPV4 channels are temperature sensitive and this is within their optimum (Güler *et al.*, 2002; Watanabe *et al.*, 2002).

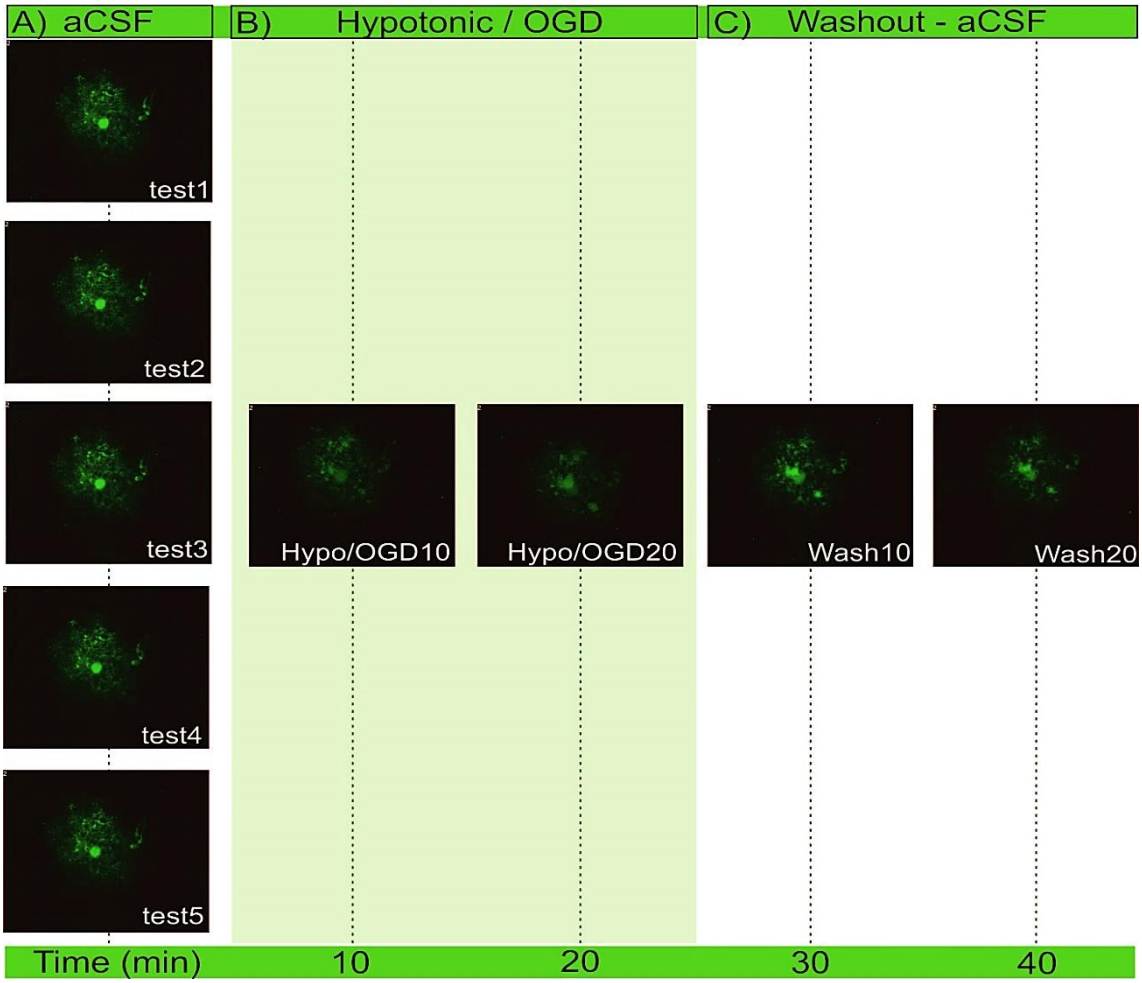

Figure 11: Schematic representation of our experimental protocol. A) At the beginnning we acquired 5 control stacks of images (tests 1 – 5) to correct photobleaching of EGFP. B) In the next phase we applied hypotonic (Hypo) or OGD solution to the brain slice for 20 minutes. We measured selected cell every 10 minutes. This was followed by a washout (Wash) phase (C), when the slices were returned to the aCSF for 20 minutes. We measured the cells every 10 minutes.

8.2.1 Hypotonicity-induced astrocyte swelling

To test our working hypothesis about astrocyte volume regulations we performed experiments in hypotonic conditions, following experimental protocol shown in Fig. 11. All groups showed an increase in the astrocytic volume after 10 minutes of application of the hypotonic solution, compared to the control measures and the volume continued to rise for another 10 minutes (Hypo20) when it reached the average volume of about 200 % of the control measurement. All the groups also decreased their volume after the washout phase, compared to the maximal swelling after 20 minutes in hypotonic solution (Fig. 12, 13).

8.2.2 Hypotonicity-induced whole-cell swelling of astrocytes from AQP4-deficient mice

We measured astrocyte volume in the acute brain slices of $AQP4^{-/-}$ mice. In total, we measured 21 cells from $AQP4^{-/-}$ mice and compared them to the values from 21 cells from control animals. Cells from $AQP4^{-/-}$ animals showed significant volume increase after 10 and 20 minutes of application of hypotonic solution (significance marks not shown, $p<0.001$), their average volume increase reached after 20 minutes of hypotonic conditions 202.53 ± 10.61 %, and similarly also showed a significant volume restoration after 10 and 20 minutes of washout phase in aCSF solution reaching 114.7 ± 10.31 % (### $p<0.001$). On the contrary, in controls the volume restoration after washout was visible, but not significant (Fig. 12A). When compared to controls, the cells from $AQP4^{-/-}$ mice showed a similar pattern of swelling as the control cells (Fig. 12A, 13).

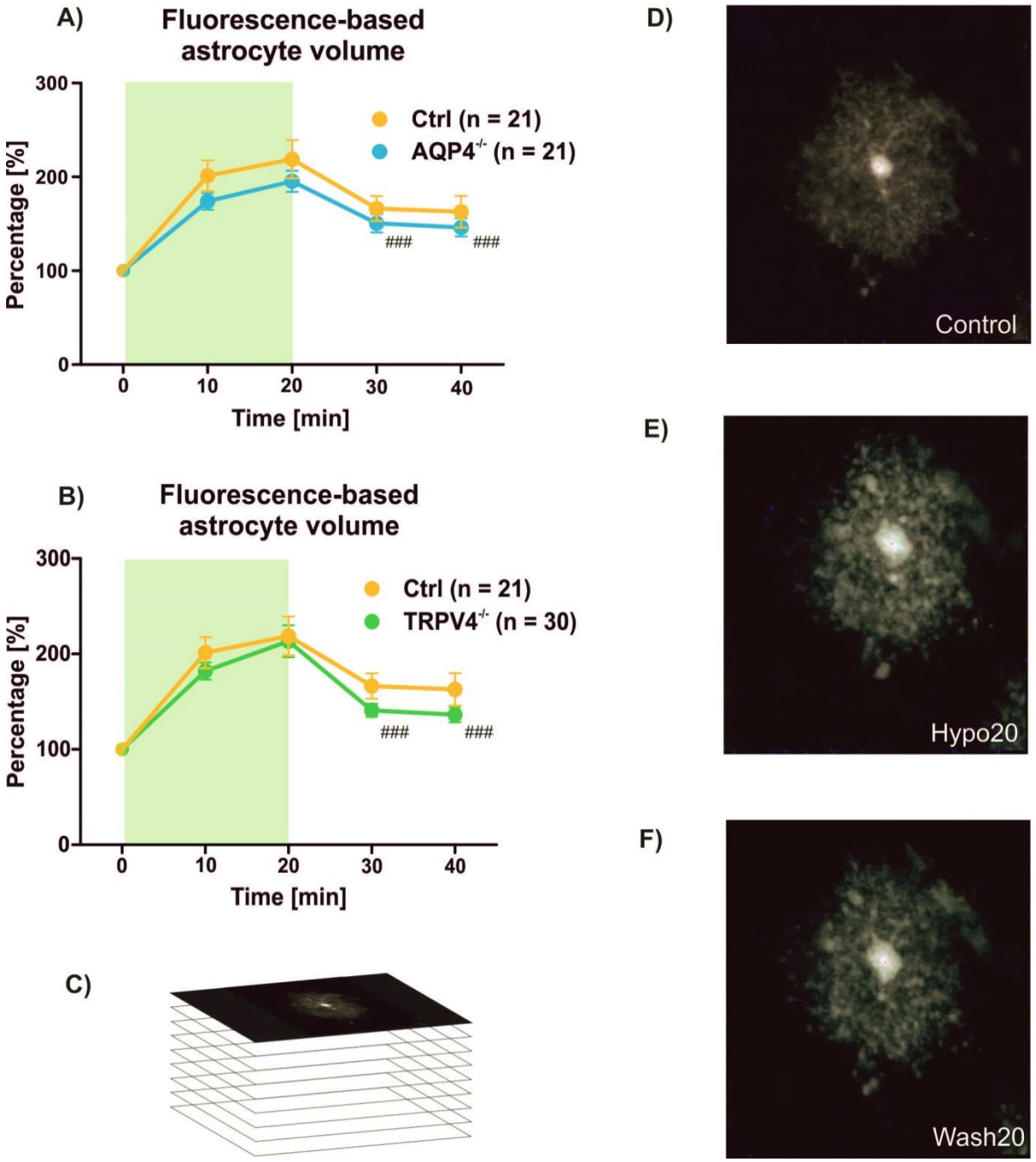

Figure 12: Hypotonicity-induced astrocyte swelling. The light green parts represent hypotonic solution application, n represents number of cells in each group. A) Astrocytes from AQP4$^{-/-}$ mice show an increase in cell volume in hypoosmotic conditions and also a significant cell volume restoration when returned to aCSF (###, $p<0.001$). The same pattern show also cells from TRPV4$^{-/-}$ mice (B). The cellular volume was measured from stacks of focal images – Z-stacks (C) with a control measurement at the beginning (D) and another four measurements every 10 minutes during hypotonic solution application and washout phase (E, F).

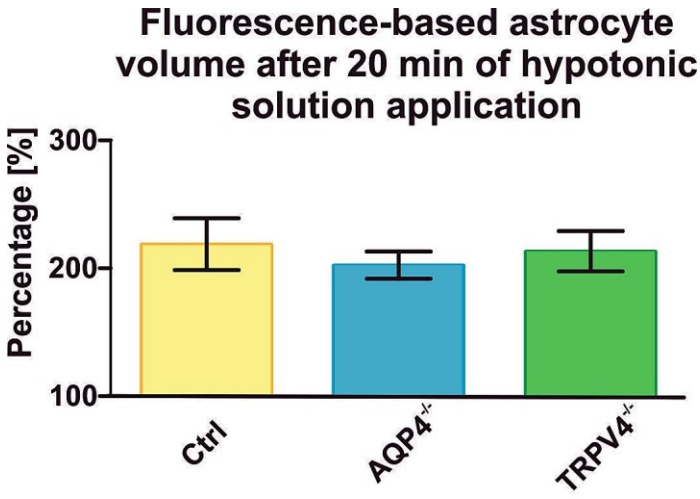

Figure 13: The average astrocyte volume reached after 20 minutes of hypotonic solution application. When compared to controls, none of the groups of cells from genetically modified animals showed any significant differences in their swelling.

8.2.3 Hypotonicity-induced whole-cell swelling of astrocytes from TRPV4-deficient mice

Similarly to AQP4$^{-/-}$, the astrocytes from TRPV4$^{-/-}$ animals swelled significantly (significance marks not shown, $p<0.001$). When compared to controls, the cells from TRPV4$^{-/-}$ mice reached about the same average volume after 20 minutes in hypotonic conditions. However, the volume increase of astrocytes from TRPV4$^{-/-}$ was slower. After 10 minutes in hypotonic solution the average volume of TRPV4$^{-/-}$ cells was slightly smaller (182.16 ± 9.01 %), than that of controls (201.31 ± 16.43 %), but not significantly. After the washout phase, the cells from TRPV4$^{-/-}$ mice decreased their volume significantly (### $p<0.001$), compared to the maximal volume after 20 minutes of hypotonic stress (Fig. 12B, 13) and the volume restoration during washout phase was the most substantial of all the groups. The difference in volume between Hypo20 and Wash20 was 77 % on average. In total, we measured the volume of 30 astrocytes from TRPV4$^{-/-}$ animals. The results obtained in TRPV4$^{-/-}$ mice were recently published in Pivonkova et al., 2018.

Taken together, the volume of the cells lacking any of the channels of our interest did not differ significantly from the control group. We can summarize that swelling as well as volume restoration of astrocytes from AQP4$^{-/-}$, TRPV4$^{-/-}$ and control mice during the hypotonic and washout phase were comparable.

8.2.4 Hypotonicity-induced volume changes of astrocytic endfeet

In the second part of our experiments, we focused on the volume changes in astrocytic endfeet, because they are specialized structures surrounding brain capillaries and create a part of BBB. On the endfeet, a high density of AQP4 was shown (Nielsen *et al.*, 1997; Furman *et al.*, 2003), with possible colocalization with TRPV4 (Benfenati *et al.*, 2011; Jo *et al.*, 2015). We measured the diameter of endfeet in all our experimental groups and from the changes of the diameter we estimated changes of the endfeet volume. In total, we measured 52 astrocytic endfeet. For our experiments, we used the same protocol, as for the measurements of whole-cell volume (Fig. 11).

In the endfeet of astrocytes from AQP4$^{-/-}$ animals (n = 24), we observed a significant volume increase in hypotonic conditions and also a significant volume decrease during the washout, when the cells were returned to aCSF. We did not find any difference between the average volume in controls and AQP4$^{-/-}$ - maximal volume of AQP4$^{-/-}$ was 155.72 ± 12.04 % and of controls was 149.89 ± 7.75 %. It is behavior very similar to the whole cells (Fig. 14A).

Similarly, also astrocytic endfeet from TRPV4$^{-/-}$ animals (n = 12) changed their volume according to the applied solution. On the contrary to the rest of our results, we found a significant difference after 10 minutes of hypotonic solution application between the astrocytic endfeet volume from control (138.40 ± 5.58 %) and TRPV4$^{-/-}$ (120.60 ± 8.20 %; *$p<0.05$) mice (Fig. 14B, 15). But after 20 minutes of hypotonic conditions, the astrocytic endfeet volume of both goups was about the same. This suggests that the maximal volume increase evoked by hypotonic stress (after 20 min) is similar to that observed in controls, but slightly delayed within first 10 min in TRPV4$^{-/-}$ when compared to controls. These results were published in Pivonkova *et al.*, 2018.

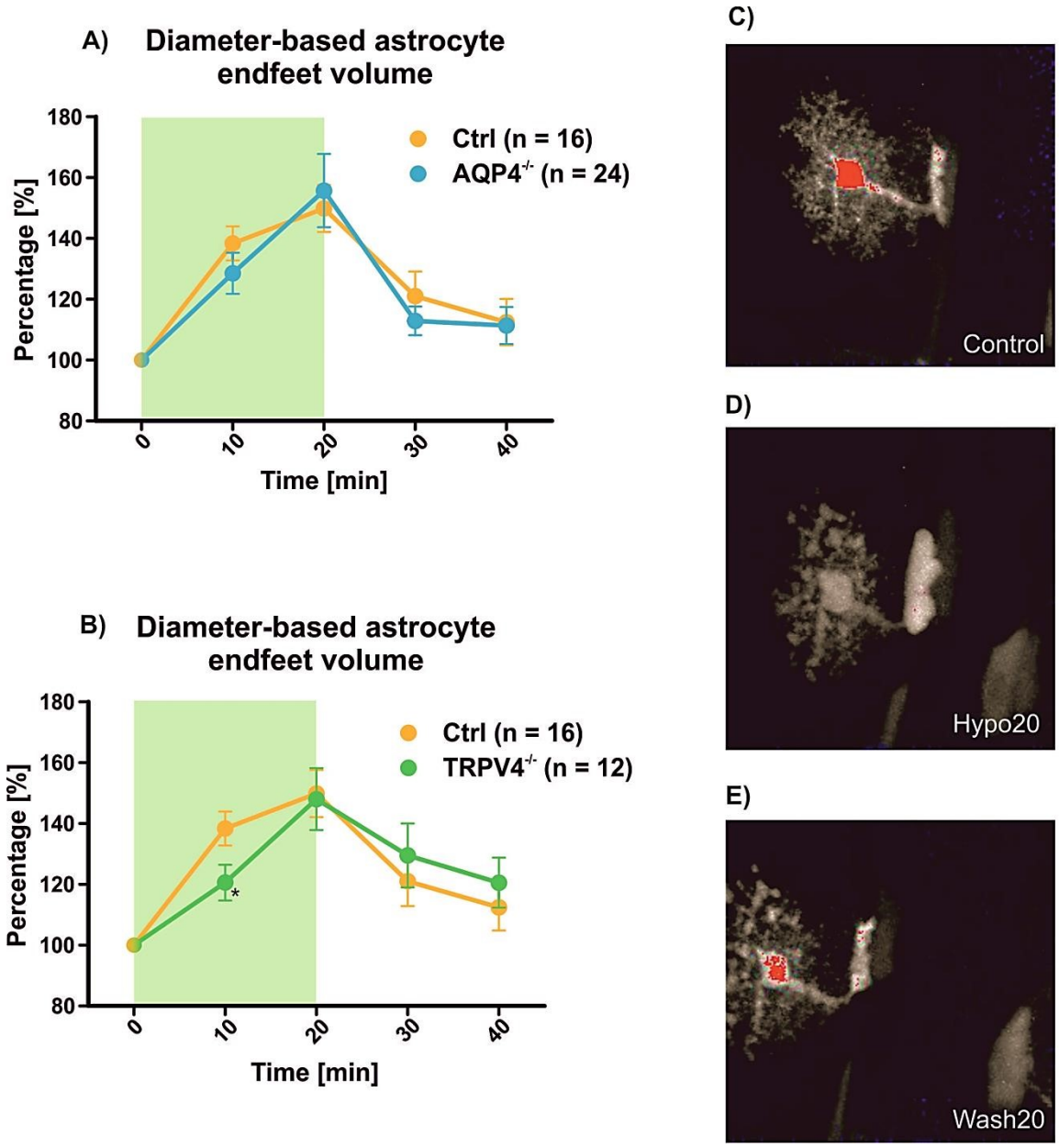

Figure 14: Hypotonicity-induced swelling of astrocytic endfeet. The light green parts represent hypotonic solution application, n represents the number of cells in each group. A) Astrocytic endfeet from AQP4$^{-/-}$ mice show an increase in their volume in hypotonic conditions and also a significant volume restoration during washout in aCSF (significance marks not shown). We did not observe any significant difference between the volume of astrocytic endfeet from AQP4$^{-/-}$ animals and those from controls. The astrocytic endfeet from TRPV4$^{-/-}$ mice showed a significantly smaller volume (*; $p<0.05$) after 10 min of hypotonic solution application when compared to controls, but in the other time points the volume ofastrocytic endfeet from TRPV4$^{-/-}$ and control animals did not differ (B). The astrocytic endfeet volume was estimated from stacks of focal images (Z-stacks) with a control measurement at the beginning (C) and another four measurements every 10 minutes during hypotonic solution application and washout (D, E).

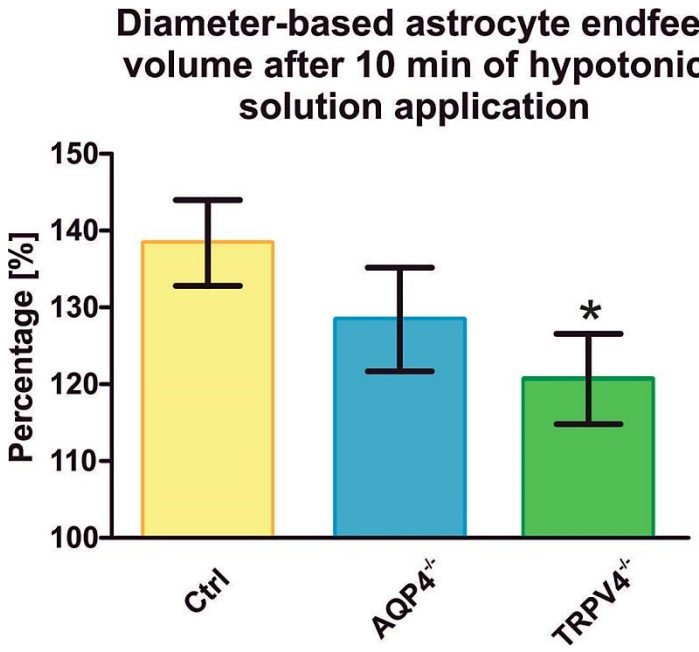

Figure 15: Hypotonicity-induced swelling of astrocytic endfeet after 10 min of hypotonic solution application. We found a significant difference between the average volume increase of astrocytic endfeet from TRPV4$^{-/-}$ mice and from control mice (*; $p<0.05$). The astrocytic endfeet from AQP4$^{-/-}$ mice did not show any difference when compared to controls.

8.2.5 OGD-induced astrocyte swelling

OGD is a well-established model of reproducible ischemia. The cells (or in our case acute brain slices) are washed with a solution similar to aCSF, but without glucose, and the OGD solution is saturated with only 5% oxygen. For the experiments, we used the same experimental protocol, as in previous experiments with the hypotonic solution (Fig. 11).

8.2.6 OGD-induced volume changes of astrocytes from AQP4-deficient animals

The quantification of volume changes in situ during the OGD application revealed significant differences between astrocytes from AQP4$^{-/-}$ and control mice. The volume changes in astrocytes from AQP4$^{-/-}$ animals were in average significantly smaller (reaching 108.75 ± 4.49 %; **p<0,01), while the average volume changes in controls were 153.99 ± 12.94 % (Fig. 16A, 17). During the washout phase astrocytes of controls partially reduced their volume, while astrocytes from AQP4$^{-/-}$ mice did not decrease their volume, but they even started to rise. After 20 minutes of washout in aCSF, the cells from AQP4$^{-/-}$ animals reached a maximal volume change of 127.63 ± 12.72 %, which was similar to that detected in

controls (135.05 ± 9.72 %, Fig. 16A). In total, we quantified volume changes in 11 cells from AQP4$^{-/-}$ animals and 19 cells from control animals.

8.2.7 OGD-induced volume changes of TRPV4-deficient astrocytes

In TRPV4$^{-/-}$ astrocytes the volume changes evoked by 20 minutes of OGD were not significantly different from those observed in controls. During OGD the average volume changes in astrocytes from TRPV4$^{-/-}$ mice reached 135.75 ± 9.42 % (Fig. 16B) and 153.99 ± 12.94 % in controls. Nevertheless, after 10 minutes of OGD we detected a slightly slower swelling in TRPV4$^{-/-}$ astrocyte (Fig. 17), however these changes were not significant. As both TRPV4$^{-/-}$ and control astrocyte showed similar volume changes during washout period, we can also conclude that TRPV4 deletion had no effect on astrocyte volume recovery. Astrocyte volume in both types of mice slowly declined during washout, reaching the average values of 131.58 ± 9.47 % (TRPV4$^{-/-}$) and 135.05 ± 9.72 % in controls (Fig. 16B). We quantified volume changes in 21 astrocytes from TRPV4$^{-/-}$ mice and the results were published by Pivonkova *et al.*, 2018.

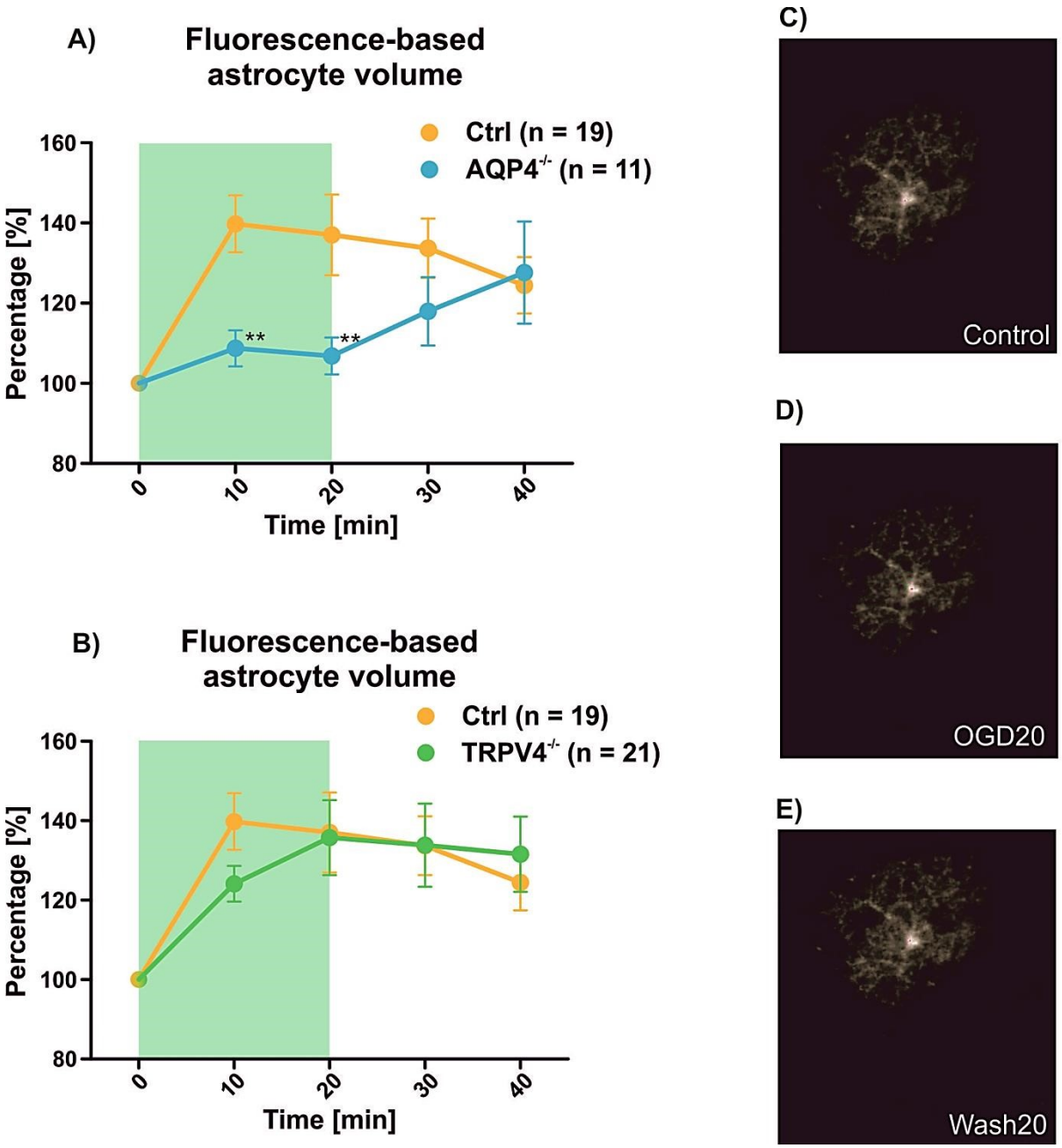

Figure 16: OGD-induced astrocyte volume changes. The light green parts represent OGD application. A) When compared to controls, the astrocytes from AQP4$^{-/-}$ mice showed a significantly smaller volume changes after OGD application (**$p<0.01$). They were also unable to restore their volume during the washout phase. On the contrary, the astrocytes from TRPV4$^{-/-}$ animals did not show any difference in their volume, when compared to controls (B). The astrocyte volume measurements followed a protocol with control measurement at the time 0 (C), which was followed by four measurements every 10 minutes during the OGD application and washout (D, E).

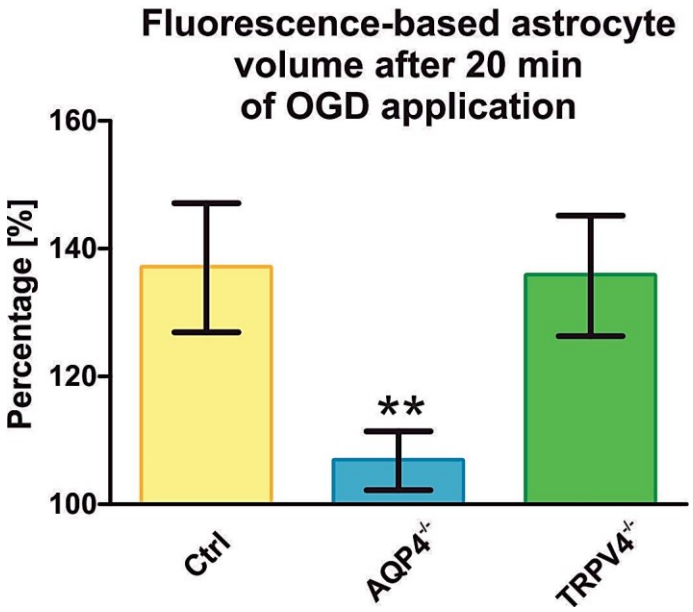

Figure 17: OGD-induced swelling of astrocytes after 20 min of OGD application. We found a significant difference between the average volume of astrocytes from AQP4$^{-/-}$ mice and from control mice (**p<0.01). The astrocytes from TRPV4$^{-/-}$ mice did not show any difference when compared to controls.

8.2.8 OGD-induced volume changes of astrocytic endfeet

We measured diameter-based volume changes of astrocytic endfeet from AQP4$^{-/-}$, TRPV4$^{-/-}$ and control animals. In total, we quantified volume chnages in 49 endfeet. For the measurements we used the same protocol as for all the other measurements (Fig. 11).

Similarly to the whole astrocytes, astrocytic AQP4$^{-/-}$ endfeet showed a significantly smaller volume changes after 20 minutes of OGD application (maximal volume 119.60 ± 5.61 %; *p<0.05), while marked volume changes were observed in endfeet of controls (150.60 ± %). However, on the contrary to the whole cells, in AQP4$^{-/-}$ mice the volume of astrocytic endfeet was restored during the washout phase. The final volume was significantly smaller in AQP4$^{-/-}$ endfeet (102.95 ± %) than the volume of controls (148.78 ± %).

Interestingly, The TRPV4$^{-/-}$ endfeet did not show any significant difference when compared to controls. They swelled during the OGD application and restored their volume during the washout, however just mildly and not significantly (Fig. 18B, 19).

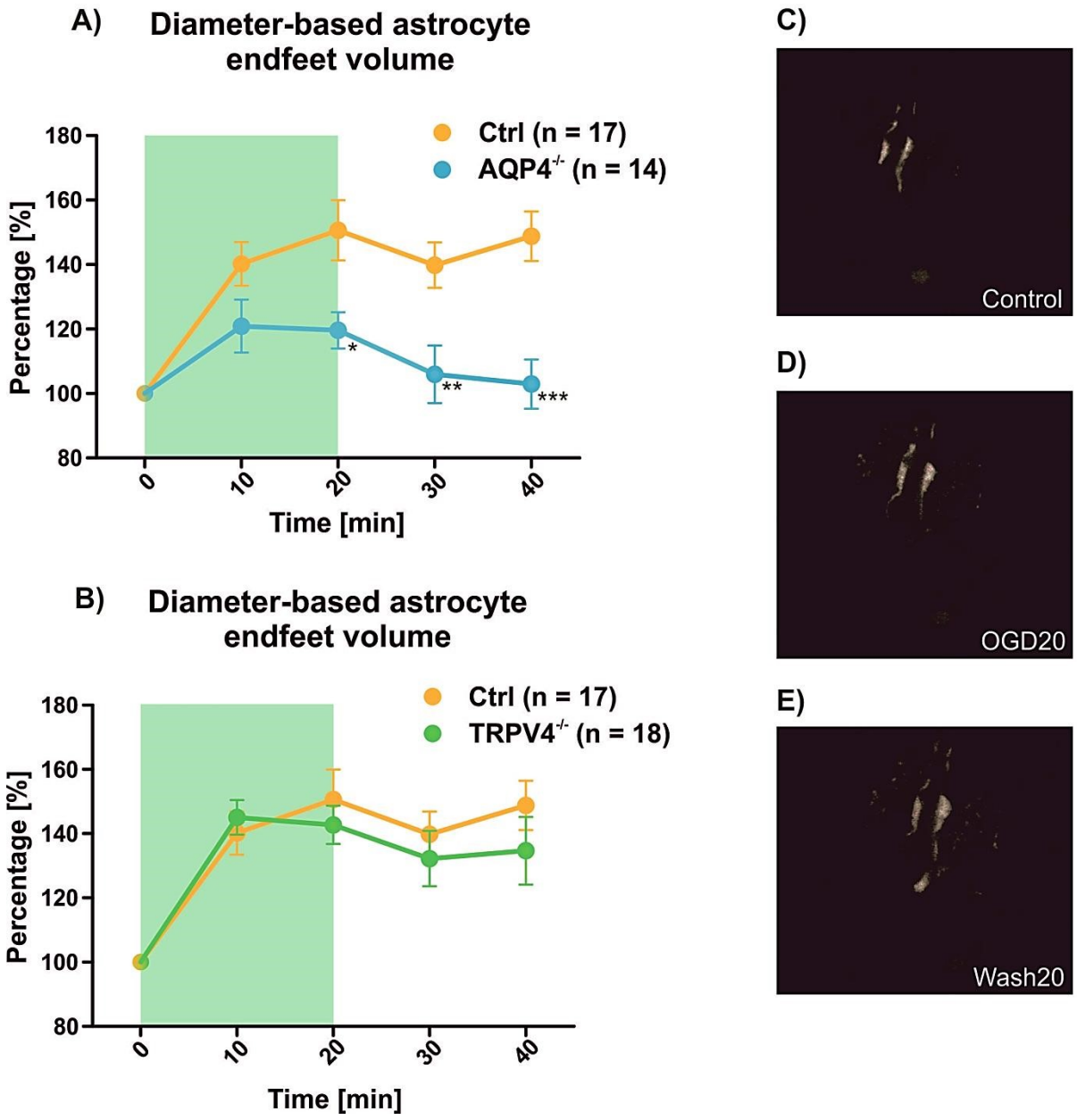

Figure 18: OGD-induced volume changes in astrocytic endfeet. The light green parts represent OGD application. A) When compared to controls, the astrocytic endfeet from AQP4$^{-/-}$ mice showed a significantly smaller volume changes after 20 min of OGD application (*$p<0.05$). They also restored their volume during the washout phase, contrary to controls (**$p<0.01$; ***$p<0.001$). The astrocytic endfeet from TRPV4$^{-/-}$ animals did not show any difference in their volume when compared to controls (B). The endfeet volume measurements followed a protocol with a control measurement at the time 0 (C), which was followed by a 20 min OGD application and 20 min washout (D, E).

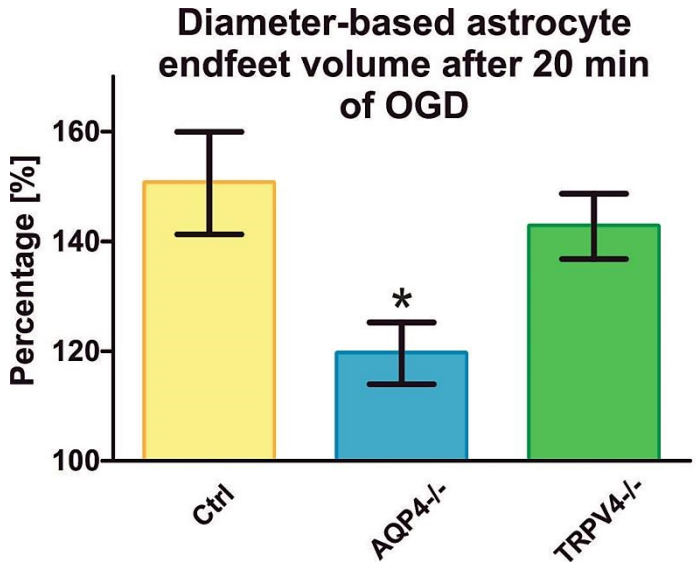

Figure 19: OGD-induced volume changes of astrocytic endfeet after 20 minutes of OGD application. The astrocytic endfeet from AQP4$^{-/-}$ mice reached a significantly smaller volume (*$p<0.05$) than the controls. The astrocytic endfeet from TRPV4$^{-/-}$ animals did not differ from the controls.

9 Discussion

In this diploma theses, we investigated the role of AQP4 and TRPV4 in astrocytic volume changes evoked by ischemia like stimuli. Based on the results of previous *in vitro* experiments (Benfenati et al., 2011) we hypothesized that both AQP4 and TRPV4 could have a protective effect against cytotoxic brain swelling and that both channels could be involved in the process of astrocytic RVD. Our results indicate that different regulatory mechanisms are involved in our models because the responses of the astrocytes from our experimental groups differ between both pathological stimuli.

9.1 Compensation of AQP4 deletion by changes in Connexin 43 localization

AQP4 is a major form of water channels in the mouse brain. Its role in brain edema formation was studied in several projects using different models of ischemic injury (Manley *et al.*, 2000; Papadopoulos and Verkman, 2005). These experiments confirmed better survival

of animals with induced ischemic injury and also the protective effect of AQP4 deletion on the size of brain edema.

In our experiments, we were able to detect swelling of astrocytes from $AQP4^{-/-}$ animals during hypoosmotic stress. The fact, that $AQP4^{-/-}$ astrocytes swell to the same level as controls, was in opposition to our hypothesis as we supposed that removing the main water pathway from the astrocytic membranes would prevent the cells from swelling. The finding that they do increase their volume indicates involvement of some compensatory mechanism, which enables water to flow through the plasmatic membrane in approximately the same amount, as the AQP4 would. One of the possible and often suggested mechanisms is Cx43 upregulation. Cx43 is astrocytic gap junctional protein, together with Cx30. These two proteins can be considered an intercellular pathways, through which water moves together with ions and small molecules. In the study of Katoozi *et al.*, 2017, deletion of AQP4 led to a significant increase in the amount of Cx43. This increase, however, was caused by the changes in posttranslational modifications rather than the upregulation of Cx43 gene transcription. On the contrary, Nicchia *et al.*, 2005 reported a decrease in the levels of Cx43 associated with AQP4 gene silencing *in vitro*. These opposing findings can be the result of different regulatory mechanisms involved in cellular function *in vitro* and *in vivo*. Also in both experiments, different methods of AQP4 deletion were engaged.

In favor of the involvement of Cx43 in the compensation of AQP4 deletion point also our results from the experiments with OGD. We used the OGD application on astrocytes to simulate properties of ischemic brain injury. Our experiments on $AQP4^{-/-}$ astrocytes revealed a significantly smaller volume of $AQP4^{-/-}$ astrocytes during OGD application, when compared to the controls. These findings are in agreement with the work of Anderova *et al.*, 2014, who performed *in situ* experiments with OGD application on α-syntrophin(α-Syn)-deficient animals and reported a significantly smaller volume of astrocytes from α-Syn-deficient animals. Similarly to our results, they did also not detect any volume decrease during the washout phase.

Obviously, different regulatory mechanisms are involved in astrocytic volume changes induced by hypoosmotic stress and by OGD. The mechanisms, which were activated during the hypoosmotic stress to compensate AQP4 deletion are obviously not functioning during OGD. While the Cx43 can possibly contribute to hypotonicity-induced astrocyte swelling, during OGD it undergoes changes that result in the lack of swelling in the

astrocytes from AQP4$^{-/-}$ mice. Wu, Yu and Feng, 2015 and Xie *et al.*, 2017 reported that during OGD Cx43 is retracted from the plasmatic membrane by endocytosis and translocated into the cytoplasm. This translocation together with AQP4 deletion can possibly result in the lack of pathways for water movement across the plasmatic membrane. It can also explain our results from AQP4$^{-/-}$ astrocytes and the fact, that the cells maintained approximately the same volume during the whole OGD application.

In our experiments, during the washout phase after the OGD application astrocytes increased their volume. The lack of RVD during reoxygenation was previously reported *in situ* by Anderova *et al.*, 2014. The finding that AQP4$^{-/-}$ astrocytes lack RVD and their volume continues to rise even in aCSF, can again be explained by the changes in Cx43 localization. In the study of Wu, Yu and Feng, 2015, a recovery of Cx43 localization on the plasmatic membrane was reported during reoxygenation after OGD. In our case, this would mean the opening of alternative pathways for water movement through plasmatic membranes and thus possibility of water influx into the astrocytes. After the Cx43 translocation back to the plasmatic membrane during the washout phase in our experiments, astrocyte volume continued to rise in agreement with the study of Anderova *et al.*, 2014.

On the contrary, our results showed a small volume increase of the astrocyte endfeet from AQP4$^{-/-}$ animals during OGD as well as a weak volume restoration during the following washout. According to the recent findings, astrocyte peripheral processes have their own local protein translation (Sakers *et al.*, 2017). It is possible that this local translation is a key player in modulation of BBB and also in modulation of regulatory mechanisms that are engaged during the pathological treatment and which differ from the mechanisms activated in cell soma.

9.2 Expression of TRPV4 channels in astrocytes

We were not able to detect any volume differences between the whole astrocytes from TRPV4$^{-/-}$ and control animals under any of the pathological stimuli we used. Our ability to detect a significant volume decrease in TRPV4$^{-/-}$ astrocytes during washout is in contrast to the results from several *in vitro* studies. Those showed that suppression or deletion of TRPV4 channels led to inhibition of RVD (Benfenati *et al.*, 2011; Hoshi *et al.*, 2018; Pivonkova *et al.*, 2018). This difference can be caused by a low level of TRPV4 expression on astrocytes. Shibasaki *et al.*, 2014 reported that only about 20 – 30 % of astrocytes do express TRPV4

channels *in vitro* and *in situ*. The same results were reported by Pivonkova *et al.*, 2018, who measured TRPV4 presence in GFAP/EGFP astrocytes. Aside from the whole cells, we also measured diameter-based volume changes of astrocytic endfeet, where the TRPV4 is abundant (Benfenati *et al.*, 2007). The only significant difference we dected between TRPV4$^{-/-}$ and control endfeet was after 10 min of hypotonic solution application when the TRPV4$^{-/-}$ endfeet reached a smaller volume than the controls. This can indicate involvement of TRPV4 channels in the speed of astrocytic volume kinetics.

On the contrary to our own results, when we were not able to detect any significant difference between control and TRPV4$^{-/-}$ astrocytes, Chmelova *et al.*, 2019 detected significantly smaller extracellular space (ECS) shrinkage *in situ* during OGD in TRPV4$^{-/-}$ animals than in controls. This is agreement with the results of Pivonkova *et al.*, 2018, who found a significantly larger lesion after permanent MCAO in TRPV4$^{-/-}$ mice, than in controls. These findings indicate that TRPV4 channels have a protective function during ischemic brain injury, however, this function is probably not associated with astrocytes only.

Since the TRPV4 channels alone do not trigger the RVD of astrocytes, they can affect astrocytic volume regulation via cooperation with other channels and transporters. These cooperations were suggested by several groups, the most often mentioned is with AQP4 (Benfenati *et al.*, 2011; Jo *et al.*, 2015; Iuso and Križaj, 2016).

9.3 Passive volume changes of cortical astrocyte

Our results of hypotonic solution application on the astrocytes or astrocyte endfeet did not reveal any significant differences in between AQP4$^{-/-}$ and control animals. The same treatment with severe hypoosmotic stress used Anderova et al., 2014 on cortical astrocytes from α-Syn-deficient mice. α-Syn is a part of the dystrophin complex which anchors AQP4 to the specific locations on a plasmatic membrane, thus its deletion results in the removal of AQP4 from plasmatic membranes (Hoddevik et al., 2017). The results of Anderova et al., 2014 indicate that deletion of α-Syn (and AQP4 removal) results in a significantly smaller volume increase of astrocytes during severe hypoosmotic stress when compared to controls. Because the hypoosmotic treatment was the same as we used, the difference in the results could be due to different data analysis. In the work of Anderova et al., 2014, a custom-made program was used for evaluating the astrocyte volume changes and they also used one month old animals. This may be the result for different outcomes. In our experiments, we quantified

the astrocyte volume based on fluorescence intensity using the ImageJ/FIJI software (Awadová et al., 2018).

Same results of reduced cellular volume of AQP4$^{-/-}$ glia obtained also Iuso and Križaj, 2016, but their measurements were performed on Müller glia in the retina and not on cortical astrocytes. It is possible that variable regulatory mechanisms are activated between these two glial types and that leads to different experimental results. On blood-retina interface, deletion of AQP4 leads to blood-retina barrier dysfunction and to astrocyte activation, which results in an inflammatory response of the retina (Nicchia *et al.*, 2016). In our mice, however, no BBB impairment was detected.

Based on the results of Benfenati *et al.*, 2011, and Anderova *et al.*, 2014, we did not expect to see any RVD in AQP4$^{-/-}$ and TRPV4$^{-/-}$ astrocytes during the washout phase in our experiments. However, our results from the experiments with hypotonic solution did show a significant volume decrease in the whole cells as well as in the astrocyte endfeet. The *in vitro* study of Benfenati *et al.*, 2011 showed, that deletion of AQP4 led to stabilization of the increased volume reached during the hypoosmotic stimulation and that AQP4 together with TRPV4 are crucial in triggering astrocyte RVD. On the contrary, the *in situ* experiments of Anderova *et al.*, 2014 revealed a mild volume reduction after long (90 min) washout even in control cells. These experiments used basically the same methods, as we did. Nevertheless, they did not detect any RVD. Interestingly, no RVD but also no difference in swelling of somata between AQP4$^{-/-}$ and control astrocytes occured after peri-infarct depolarization *in vivo* (Rakers, Schmid and Petzold, 2017).

Our findings of immediate volume response to osmotic changes are in agreement with Risher, Andrew and Kirov, 2009. They suggested that osmotically-induced volume changes in astrocytes are passive and do not include any active processes, such as RVD. In that case, volume changes are a result of passive water flow through plasmatic membrane driven by osmotic gradients.

Since astrocytes are the biggest population of glial cells in brain and are strongly involved in maintenance of brain homeostasis, any active volume regulations would possibly show not only on astrocytes themselves, but also on the changed parameters of ECS. Chmelova *et al.*, 2019 measured ECS volume in mouse brain during severe hypoosmotic stress and found no difference between the ECS volume between AQP4$^{-/-}$ and control mice.

This finding contributes to the hypothesis, that the astrocyte volume changes occuring during hypoosmotic stress are passive.

10 Conclusions

In summary, our findings suggest that AQP4 deletion leads to an activation of compensatory mechanisms, which allow water transport through plasmatic membranes of astrocytes. We hypothesize that this compensation is accomplished by changes in Cx43 posttranslational modifications, which result in an increased concentration of Cx43 channels on astrocytic membranes. On the contrary, the deletion of TRPV4 from astrocytes did not affect the swelling of astrocytes and we did not detect any changes that would indicate activation of any compensatory mechanisms. We therefore believe that TRPV4 might serve a protective effect during ischemic brain injury, however, this effect is probably not associated with astrocytes. Moreover, in our experiments we were unable to detect any active volume changes, such as RVD. Therefore we believe that volume changes of astrocytes induced by pathological stimuli are passive and that RVD is an attribute of cultured cells only.

11 References

Agre, P. *et al.* (2002) 'Aquaporin water channels-from atomic structure to clinical medicine.', *The Journal of physiology*, 542(Pt 1), pp. 3–16. doi: 10.1113/jphysiol.2002.020818.

Agre, P. (2006) 'The Aquaporin Water Channels', *Proceedings of the American Thoracic Society*, 3, pp. 5–13. doi: 10.1513/pats.200510-109JH.

Akdemir, G. *et al.* (2014) 'Neuroprotective effect of aquaporin-4 deficiency in a mouse model of severe global cerebral ischemia produced by transient 4-vessel occlusion', *Neuroscience Letters*, (547), pp. 70–75. doi: 10.1086/498510.

Alliot, F., Godin, I. and Pessac, B. (1999) 'Microglia derive from progenitors, originating from the yolk sac, and which proliferate in the brain', *Developmental Brain Research*, 117(2), pp. 145–152. doi: 10.1016/S0165-3806(99)00113-3.

Almeida, R. G. *et al.* (2011) 'Individual axons regulate the myelinating potential of single oligodendrocytes in vivo', *Development*, 138(20), pp. 4443–4450. doi: 10.1242/dev.071001.

Anderova, M. *et al.* (2014) 'Altered astrocytic swelling in the cortex of α-syntrophin-negative GFAP/EGFP MICE', *PLoS ONE*, 9(11), pp. 1–34. doi: 10.1371/journal.pone.0113444.

Anders, S. *et al.* (2014) 'Spatial properties of astrocyte gap junction coupling in the rat hippocampus', *Philosophical Transactions of the Royal Society B: Biological Sciences*, 369(1654), pp. 20130600–20130600. doi: 10.1098/rstb.2013.0600.

Armbruster, M., Hanson, E. and Dulla, C. G. (2016) 'Glutamate Clearance Is Locally Modulated by Presynaptic Neuronal Activity in the Cerebral Cortex', *The Journal of Neuroscience*, 36(40), pp. 10404–10415. doi: 10.1523/JNEUROSCI.2066-16.2016.

Arniges, M. *et al.* (2006) 'Human TRPV4 channel splice variants revealed a key role of ankyrin domains in multimerization and trafficking', *Journal of Biological Chemistry*, 281(3), pp. 1580–1586. doi: 10.1074/jbc.M511456200.

Awadová, T. *et al.* (2018) 'Cell volume changes as revealed by fluorescence microscopy: Global vs local approaches', *Journal of Neuroscience Methods*, 306, pp. 38–44. doi: 10.1016/j.jneumeth.2018.05.026.

Bacigaluppi, M., Comi, G. and Hermann, D. M. (2010) 'Animal models of ischemic stroke. Part two: modeling cerebral ischemia.', *The open neurology journal*, 4, pp. 34–38. doi: 10.2174/1874205X01004020034.

Baethmann, A. (1978) 'Pathophysiological and pathochemical aspects of cerebral edema', *Neurosurgical Review*, 1, pp. 85–100. Available at: http://link.springer.com/article/10.1007/BF01646721.

Becker, D. *et al.* (2008) 'The C-terminal domain of TRPV4 is essential for plasma membrane localization', *Molecular Membrane Biology*, 25(2), pp. 139–151. doi: 10.1080/09687680701635237.

De Bellis, M. *et al.* (2017) 'Translational readthrough generates new astrocyte AQP4 isoforms that modulate supramolecular clustering, glial endfeet localization, and water transport', *Glia*, 65(5), pp. 790–803. doi: 10.1002/glia.23126.

Benfenati, V. *et al.* (2007) 'Expression and functional characterization of transient receptor potential vanilloid-related channel 4 (TRPV4) in rat cortical astrocytes', *Neuroscience*, 148(4), pp. 876–892. doi: 10.1016/j.neuroscience.2007.06.039.

Benfenati, V. *et al.* (2011) 'An aquaporin-4/transient receptor potential vanilloid 4 (AQP4/TRPV4) complex is essential for cell-volume control in astrocytes.', *Proceedings of the National Academy of Sciences of the United States of America*, 108(6), pp. 2563–2568. doi: 10.1073/pnas.1012867108.

Berdichevsky, E. *et al.* (1983) 'Kainate, N-methylaspartate and other excitatory amino acids increase calcium influx into rat brain cortex cells in vitro', *Neuroscience Letters*, 36(1), pp. 75–80. doi: 10.1016/0304-3940(83)90489-5.

Brambilla, R. *et al.* (2009) 'Transgenic inhibition of astroglial NF-κB leads to increased axonal sparing and sprouting following spinal cord injury', *The Journal of Neurochemistry*, 110(2), pp. 765–778. doi: 10.1111/j.1471-4159.2009.06190.x.Transgenic.

Busch, E. *et al.* (1996) 'Potassium-induced cortical spreading depressions during focal cerebral ischemia in rats: Contribution to lesion growth assessed by diffusion-weighted NMR and biochemical imaging', *Journal of Cerebral Blood Flow and Metabolism*, 16(6), pp. 1090–1099. doi: 10.1097/00004647-199611000-00002.

Butenko, O. *et al.* (2012) 'The increased activity of TRPV4 channel in the astrocytes of the adult rat hippocampus after cerebral Hypoxia/Ischemia', *PLoS ONE*, 7(6), p. e39959. doi: 10.1371/journal.pone.0039959.

Cahoy, J. D. *et al.* (2008) 'A Transcriptome Database for Astrocytes , Neurons , and Oligodendrocytes : A New Resource for Understanding Brain Development and Function', 28(1), pp. 264–278. doi: 10.1523/JNEUROSCI.4178-07.2008.

Camassa, L. M. A. *et al.* (2015) 'Mechanisms underlying AQP4 accumulation in astrocyte endfeet', *Glia*, 63(11), pp. 2073–2091. doi: 10.1002/glia.22878.

Carloni, S. *et al.* (2007) 'Extended role of necrotic cell death after hypoxia-ischemia-induced neurodegeneration in the neonatal rat', *Neurobiology of Disease*, 27(3), pp. 354–361. doi: 10.1016/j.nbd.2007.06.009.

Cheng, Y. *et al.* (1998) 'Caspase inhibitor affords neuroprotection with delayed administration in a rat model of neonatal hypoxic-ischemic brain injury', *Journal of Clinical Investigation*, 101(9), pp. 1992–1999. doi: 10.1172/JCI2169.

Chmelova, M. *et al.* (2019) 'The role of aquaporin-4 and transient receptor potential vaniloid isoform 4 channels in the development of cytotoxic edema and associated extracellular diffusion parameter changes', *European Journal of Neuroscience*, (Jan 11). doi: 10.1111/ejn.14338.

Choi, D. W. (1988) 'Glutamate neurotoxicity and diseases of the nervous system', *Neuron*, 1(8), pp. 623–634. doi: 10.1016/0896-6273(88)90162-6.

Chvátal, A., Anděrová, M. and Kirchhoff, F. (2007) 'Three-dimensional confocal morphometry – a new approach for studying dynamic changes in cell morphology in brain slices', *Journal of Anatomy*, 210(6), pp. 671–683. doi: 10.1111/j.1469-7580.2007.00724.x.

Clapham, D. E., Runnels, L. W. and Strübing, C. (2001) 'The TRP ion channel family', *Nature Reviews Neuroscience*, 2(6), pp. 387–396. doi: 10.1038/35077544.

Cornell-Bell, A. H. *et al.* (1990) 'Glutamate induces calcium waves in cultured astrocytes: long- range glial signalling', *Science*, 247(4941), pp. 470–473. PMID: 1967852.

Dawson, M. R. L. *et al.* (2003) 'NG2-expressing glial progenitor cells: An abundant and widespread population of cycling cells in the adult rat CNS', *Molecular and Cellular Neuroscience*, 24(2), pp. 476–488. doi: 10.1016/S1044-7431(03)00210-0.

Deng, Z. *et al.* (2018) 'Cryo-EM and X-ray structures of TRPV4 reveal insight into ion permeation and gating mechanisms', *Nature Structural and Molecular Biology*, 25(3), pp. 252–260. doi: 10.1038/s41594-018-0037-5.Cryo-EM.

Dijkhuizen, R. M. *et al.* (1999) 'Correlation between tissue depolarizations and damage in focal ischemic rat brain', *Brain Research*, 840(1–2), pp. 194–205. doi: 10.1016/S0006-8993(99)01769-2.

Dunn, K. M. *et al.* (2013) 'TRPV4 channels stimulate Ca2+-induced Ca2+ release in astrocytic endfeet and amplify neurovascular coupling responses', *Proceedings of the National Academy of Sciences*, 110(15), pp. 6157–6162. doi: 10.1073/pnas.1216514110.

Durukan, A. and Tatlisumak, T. (2007) 'Acute ischemic stroke: Overview of major experimental rodent models, pathophysiology, and therapy of focal cerebral ischemia', *Pharmacology Biochemistry and Behavior*, 87(1), pp. 179–197.
doi: 10.1016/j.pbb.2007.04.015.

Fan, Y. *et al.* (2013) 'Aquaporin-4 promotes memory consolidation in Morris water maze', *Brain Structure and Function*, 218(1), pp. 39–50. doi: 10.1007/s00429-011-0373-2.

Faulkner, J. R. *et al.* (2004) 'Reactive Astrocytes Protect Tissue and Preserve Function after Spinal Cord Injury', *Journal of Neuroscience*, 24(9), pp. 2143–2155. doi: 10.1523/JNEUROSCI.3547-03.2004.

Feetham, C. H. *et al.* (2015) 'TRPV4 and KCa ion channels functionally couple as osmosensors in the paraventricular nucleus', *British Journal of Pharmacology*, 172(7), pp. 1753–1768. doi: 10.1111/bph.13023.

Fenske, A. R. and Prioleau, G. R. (1978) 'Clearance of edema fluid into cerebrospinal fluid', *J Neurosurg*, 48, pp. 754–764. doi: 10.3171/jns.1978.48.5.0754.

Fishman, R. A. (1975) 'Brain edema', *The New England journal of medicine*, 239(14), pp. 706–711. doi: 10.1056/NEJM197510022931407.

Fluri, F., Schuhmann, M. K. and Kleinschnitz, C. (2015) 'Animal models of ischemic stroke and their application in clinical research', *Drug Design, Development and Therapy*, 9, pp. 3445–3454. doi: 10.2147/DDDT.S56071.

Furman, C. S. *et al.* (2003) 'Aquaporin-4 square array assembly: opposing actions of M1 and M23 isoforms.', *Proceedings of the National Academy of Sciences of the United States of America*, 100(23), pp. 13609–13614. doi: 10.1073/pnas.2235843100.

Garcia-Elias, A. *et al.* (2013) 'Phosphatidylinositol-4,5-biphosphate-dependent rearrangement of TRPV4 cytosolic tails enables channel activation by physiological stimuli', *Proceedings of the National Academy of Sciences*, 110(23), pp. 9553–9558. doi: 10.1073/pnas.1220231110.

Ginhoux, F. *et al.* (2010) 'Fate Mapping Analysis Reveals That Adult Microglia Derive from Primitive Macrophages', *Science*, 330(6005), pp. 841–845. doi: 10.1126/science.1194637.Fate.

Giulian, D. and Baker, T. I. (1985) 'Peptides released by ameboid microglia regulate astroglial proliferation', *Journal of Cell Biology*, 101(6), pp. 2411–2415. doi: 10.1083/jcb.101.6.2411.

Güler, A. D. *et al.* (2002) 'Heat-Evoked Activation of the Ion Channel, TRPV4', *Journal of Neuroscience*, 22(15), pp. 6408–6414. doi: 20026679.

Harraz, O. F. *et al.* (2018) 'PIP2 depletion promotes TRPV4 channel activity in mouse brain capillary endothelial cells', *eLife*, 7(c), pp. 1–4. doi: 10.7554/eLife.38689.

Hatashita, S., Hoff, J. T. and Salamat, S. M. (1988) 'Ischemic brain edema and the osmotic gradient between blood and brain', *Journal of Cerebral Blood Flow and Metabolism*, pp. 552–559. doi: 10.1038/jcbfm.1988.96.

Herculano-Houzel, S. (2014) 'The glia/neuron ratio: How it varies uniformly across brain structures and species and what that means for brain physiology and evolution', *Glia*, 62(9), pp. 1377–1391. doi: 10.1002/glia.22683.

Hirt, L. *et al.* (2016) 'Improved long-term outcome after transient cerebral ischemia in aquaporin-4 knockout mice.', *Journal of cerebral blood flow and metabolism : official journal of the International Society of Cerebral Blood Flow and Metabolism*, pp. 1–14. doi: 10.1177/0271678X15623290.

Hoddevik, E. H. *et al.* (2017) 'Factors determining the density of AQP4 water channel molecules at the brain–blood interface', *Brain Structure and Function*, 222(4), pp. 1753-1766. doi: 10.1007/s00429-016-1305-y.

Honsa, P. *et al.* (2016) 'Generation of reactive astrocytes from NG2 cells is regulated by sonic hedgehog', *Glia*, 64(9), pp. 1518–1531. doi: 10.1002/glia.23019.

Hoshi, Y. *et al.* (2018) 'Ischemic Brain Injury Leads to Brain Edema via Hyperthermia-Induced TRPV4 Activation', *Journal of Neuroscience*, 38(25), pp. 5700–5709. doi: 10.1523/JNEUROSCI.2888-17.2018.

Huang, W. *et al.* (2014) 'Novel NG2-CreERT2 knock-in mice demonstrate heterogeneous differentiation potential of NG2 glia during development', *Glia*, 62(6), pp. 896–913. doi: 10.1002/glia.22648.

Ikeshima-kataoka, H. *et al.* (2013) 'Molecular and Cellular Neuroscience Immunological function of aquaporin-4 in stab-wounded mouse brain in concert with a pro-in fl ammatory cytokine inducer , osteopontin', *Molecular and Cellular Neuroscience*. Elsevier Inc., 56, pp. 65–75. doi: 10.1016/j.mcn.2013.02.002.

Iuso, A. and Križaj, D. (2016) 'TRPV4-AQP4 interactions "turbocharge" astroglial sensitivity to small osmotic gradients', *Channels*. Taylor & Francis, 10(3), pp. 172–174. doi: 10.1080/19336950.2016.1140956.

Jessen, K. R. (2004) 'Glial cells', *International Journal of Biochemistry and Cell Biology*, 36(10), pp. 1861–1867. doi: 10.1016/j.biocel.2004.02.023.

Jeuregui-Huerta, F. *et al.* (2010) 'Responses of glial cells to stress and glucocorticoids', *Current Immunology Review*, 6(3), pp. 195–204.
doi: 10.2174/157339510791823790.Responses.

Jie, P. *et al.* (2015) 'Activation of transient receptor potential vanilloid 4 induces apoptosis in hippocampus through downregulating PI3K/Akt and upregulating p38 MAPK signaling pathways', *Cell Death and Disease*, 6(6), p. e1775. doi: 10.1038/cddis.2015.146.

Jie, P. *et al.* (2015) 'Blockage of transient receptor potential vanilloid 4 inhibits brain edema in middle cerebral artery occlusion mice', *Frontiers in Cellular Neuroscience*, 9(April), pp. 1–6. doi: 10.3389/fncel.2015.00141.

Jo, A. O. *et al.* (2015) 'TRPV4 and AQP4 Channels Synergistically Regulate Cell Volume and Calcium Homeostasis in Retinal Műller Glia', *Journal of Neuroscience*, 35(39), pp. 13525–13537. doi: 10.1523/JNEUROSCI.1987-15.2015.

Kaneko, D., Nakamura, N. and Ogawa, T. (1985) 'Cerebral infarction in rats using homologous blood emboli: development of a new experimental model', *Stroke*, 16(1), pp. 76–84. doi: 10.1161/01.STR.16.1.76.

Kang, S. H. *et al.* (2010) 'NG2+ CNS glial progenitors remain committed to the oligodendrocyte lineage in postnatal life and following neurodegeneration', *Neuron*, 68(4), pp. 668–681. doi: 10.1016/j.neuron.2010.09.009.NG2.

Kanju, P. and Liedtke, W. (2016) 'Pleiotropic function of TRPV4 ion channels in the central nervous system', *Experimental Physiology*, 101(12), pp. 1472–1476. doi: 10.1113/EP085790.

Katada, R. *et al.* (2014) 'Greatly improved survival and neuroprotection in aquaporin-4-knockout mice following global cerebral ischemia', *FASEB Journal*, 28(2), pp. 705–714. doi: 10.1096/fj.13-231274.

Katoozi, S. *et al.* (2017) 'Targeted deletion of Aqp4 promotes the formation of astrocytic gap junctions', *Brain Structure and Function*, 222(9), pp. 3959–3972. doi: 10.1007/s00429-017-1448-5.

Kenny, A., Plank, M. J. and David, T. (2018) 'The role of astrocytic calcium and TRPV4 channels in neurovascular coupling', *Journal of Computational Neuroscience*, 44(1), pp. 97–114. doi: 10.1007/s10827-017-0671-7.

Kitchen, P. *et al.* (2016) 'Structural determinants of oligomerization of the aquaporin-4 channel', *Journal of Biological Chemistry*, 291(13), pp. 6858–6871. doi: 10.1074/jbc.M115.694729.

Klatzo, I. (1987) 'Pathophysiological aspects of brain edema', *Acta Neuropathologica*, 72, pp. 236–239. doi: 10.1016/0303-8467(84)90069-6.

Klatzo, I. (1994) 'Evolution of brain edema concepts', *Acta Neurochirurgica Supplement (Wien)*, 60, pp. 3–6. PMID: 7976571.

Knot, H. J., Zimmermann, P. A. and Nelson, M. T. (1996) 'Extracellular K+-induced hyperpolarizations and dilatations of rat coronary and cerebral arteries involve inward rectifier K+ channels', *Journal of Physiology*, 492(2), pp. 419–430. doi: 10.1113/jphysiol.1996.sp021318.

Kondo, T. and Raff, M. C. (2000) 'Oligodendrocyte precursor cells reprogrammed to become multipotent stem cells', *Science*, 289(September 2000), pp. 1754–1757. doi: 10.1126/science.289.5485.1754.

Kong, H. *et al.* (2014) 'Aquaporin-4 Knockout Exacerbates Corticosterone-Induced Depression by Inhibiting Astrocyte Function and Hippocampal Neurogenesis', *CNS Neuroscience and Therapeutics*, 20(5), pp. 391–402. doi: 10.1111/cns.12222.

Krupenko, S. A. (2009) 'FDH: an Aldehyde Dehydrogenase Fusion Enzyme in Folate Metabolism', *Chemico-Biological Interactions*, 178(1–3), pp. 84–93. doi: 10.1016/j.cbi.2008.09.007.FDH.

Lafrenaye, A. D. and Simard, J. M. (2019) 'Bursting at the Seams : Molecular Mechanisms Mediating Astrocyte Swelling', *International Journal of Molecular Sciences*, 20, p. 330. doi: 10.3390/ijms20020330.

Le, H. T. *et al.* (2014) 'Gap junction intercellular communication mediated by connexin43 in astrocytes is essential for their resistance to oxidative stress', *Journal of Biological Chemistry*, 289(3), pp. 1345–1354. doi: 10.1074/jbc.M113.508390.

Lennon, V. A. *et al.* (2005) 'IgG marker of optic-spinal multiple sclerosis binds to the aquaporin-4 water channel', *The Journal of Experimental Medicine*, 202(4), pp. 473–477. doi: 10.1084/jem.20050304.

Liddelow, S. A. *et al.* (2017) 'Neurotoxic reactive astrocytes are induced by activated microglia', *Nature*, 541(7638), pp. 481–487. doi: 10.1038/nature21029.Neurotoxic.

Liedtke, W. and Friedman, J. M. (2003) 'Abnormal osmotic regulation in trpv4-/- mice', *Proceedings of the National Academy of Sciences of the United States of America*, 100(23), pp. 13698–13703. doi: 10.1073/pnas.1735416100.

Linnik, M. D. et al. (1993) 'Evidence supporting a role for programmed cell death in focal cerebral ischemia in rats', *Stroke*, 24(ischemia, apoptosis), pp. 2002–2009. PMID: 8248983.

Lipski, J. *et al.* (2006) 'Involvement of TRP-like channels in the acute ischemic response of hippocampal CA1 neurons in brain slices', *Brain Research*, 1077(1), pp. 187–199. doi: 10.1016/j.brainres.2006.01.016.

Lisjak, M. *et al.* (2017) 'AQP4e-based orthogonal arrays regulate rapid cell volume changes in astrocytes.', *Journal of Neuroscience*, c, pp. 0776-17. doi: 10.1523/JNEUROSCI.0776-17.2017.

Liu, F. and McCullough, L. D. (2011) 'Middle cerebral artery occlusion model in rodents: Methods and potential pitfalls', *Journal of Biomedicine and Biotechnology*, 2011. doi: 10.1155/2011/464701.

Liu, M. *et al.* (2018) 'TRPV4 Inhibition Improved Myelination and Reduced Glia Reactivity and Inflammation in a Cuprizone-Induced Mouse Model of Demyelination', *Frontiers in Cellular Neuroscience*, 12(November), pp. 1–12. doi: 10.3389/fncel.2018.00392.

Liu, X. *et al.* (2008) 'Lack of sex-linked differences in cerebral edema and aquaporin-4 expression after experimental stroke', *Journal of Cerebral Blood Flow and Metabolism*, 28(12), pp. 1898–1906. doi: 10.1038/jcbfm.2008.83.Lack.

Liu, Y. *et al.* (2002) 'Oligodendrocyte and astrocyte development in rodents: An in situ and immunohistological analysis during embryonic development', *Glia*, 40(1), pp. 25–43. doi: 10.1002/glia.10111.

Maglione, M. *et al.* (2010) 'Oligodendrocytes in mouse corpus callosum are coupled via gap junction channels formed by Connexin47 and Connexin32', *Glia*, 58(9), pp. 1104–1117. doi: 10.1002/glia.20991.

Magnotti, L. M., Goodenough, D. a and Paul, D. L. (2011) 'Functional Heterotypic Interactions Between Astrocyte and Oligodendrocyte Connexins', *Glia*, 59(1), pp. 26–34. doi: 10.1002/glia.21073.Functional.

Manley, G. T. *et al.* (2000) 'Aquaporin-4 deletion in mice reduces brain edema after acute water intoxication and ischemic stroke.', *Nature medicine*, 6(2), pp. 159–163. doi: 10.1038/72256.

Manley, G. T. *et al.* (2004) 'New insights into water transport and edema in the central nervous system from phenotype analysis of aquaporin-4 null mice', *Neuroscience*, 129(4), pp. 983–991. doi: 10.1016/j.neuroscience.2004.06.088.

McBean, D. E. and Kelly, P. A. T. (1998) 'Rodent models of global cerebral ischemia: A comparison of two-vessel occlusion and four-vessel occlusion', *General Pharmacology*, 30(4), pp. 431–434. doi: 10.1016/S0306-3623(97)00284-X.

Mensch, S. *et al.* (2015) 'Synaptic vesicle release regulates the number of myelin sheaths made by individual oligodendrocytes in vivo', *Nature neuroscience*, 18(5), pp. 628–630. doi: 10.1038/nn.3991.Synaptic.

Mies, G., Iijima, T. and Hossmann, K. A. (1993) 'Correlation between Peri-infarct DC Shifts and Ischaemic Neuronal Damage in Rat', *NeuroReport*, 4, pp. 709–7011. doi: 10.1097/00001756-199306000-00027.

Miller, R. H. and Raff, M. C. (1984) 'Fibrous and protoplasmic astrocytes are biochemically and developmentally distinct', *The Journal of Neuroscience*, 4(2), pp. 585–592. doi: https://doi.org/10.1523/JNEUROSCI.04-02-00585.1984

Mola, M. G. *et al.* (2017) 'The Speed of Swelling Kinetics Modulates Cell Volume Regulation and Calcium Signaling in Astrocytes: A Different Point of View on the Role of Aquaporins', *Glia*, 64(1), pp. 139–154. doi: 10.1002/glia.22921.The.

Morales-Mulia, S. *et al.* (1998) 'Osmotic swelling-induced changes in cytosolic calcium do not affect regulatory volume decrease in rat cultured suspended cerebellar astrocytes.', *Journal of Neurochemistry*, 71, pp. 2330–2338. doi: 10.1046/j.1471-4159.1998.71062330.x

Morizawa, Y. M. *et al.* (2017) 'Reactive astrocytes function as phagocytes after brain ischemia via ABCA1-mediated pathway', *Nature Communications*, 8(1). doi: 10.1038/s41467-017-00037-1.

Mulligan, S. J. and MacVicar, B. A. (2004) 'Calcium transients in astrocyte endfeet cause cerebrovascular constrictions', *Nature*, 431(7005), pp. 195–199. doi: 10.1038/nature02827.

Nakajima, K. *et al.* (2001) 'Neurotrophin secretion from cultured microglia', *Journal of Neuroscience Research*, 65(4), pp. 322–331. doi: 10.1002/jnr.1157.

Neely, J. D. *et al.* (1999) 'Heterotetrameric composition of aquaporin-4 water channels', *Biochemistry*, 38(34), pp. 11156–11163. doi: 10.1021/bi990941s.

Neely, J. D. *et al.* (2001) 'Syntrophin-dependent expression and localization of Aquaporin-4 water channel protein', *Proceedings of the National Academy of Sciences of the United States of America*, 98(24), pp. 14108–14113. doi: 10.1073/pnas.241508198.

Nicchia, G. P. *et al.* (2005) 'New possible roles for aquaporin-4 in astrocytes: cell cytoskeleton and functional relationship with connexin43', *The FASEB Journal*, 19(12), pp. 1674–1676. doi: 10.1096/fj.04-3281fje.

Nicchia, G. P. *et al.* (2010) 'Higher order structure of aquaporin-4', *Neuroscience*. Elsevier Inc., 168(4), pp. 903–914. doi: 10.1016/j.neuroscience.2010.02.008.

Nicchia, G. P. *et al.* (2016) 'Glio-vascular modifications caused by Aquaporin-4 deletion in the mouse retina', *Experimental Eye Research*. Elsevier Ltd, 146, pp. 259–268. doi: 10.1016/j.exer.2016.03.019.

Nielsen, S. *et al.* (1997) 'Specialized membrane domains for water transport in glial cells: high-resolution immunogold cytochemistry of aquaporin-4 in rat brain.', *The Journal of Neuroscience*, 17(1), pp. 171–180. Available at: http://www.ncbi.nlm.nih.gov/pubmed/8987746.

Nilius, B. and Voets, T. (2013) 'The puzzle of TRPV4 channelopathies', *EMBO Reports*. Nature Publishing Group, 14(2), pp. 152–163. doi: 10.1038/embor.2012.219.

Nimmerjahn, A., Kirchhoff, F. and Helmchen, F. (2005) 'Neuroscience: Resting microglial cells are highly dynamic surveillants of brain parenchyma in vivo', *Science*, 308(5726), pp. 1314–1318. doi: 10.1126/science.1110647.

Nolte, C. *et al.* (1996) 'Complement 5a controls motility of murine microglial cells in vitro via activation of an inhibitory G-protein and the rearrangement of the actin cytoskeleton', *Neuroscience*, 73(4), pp. 1091–1107. doi: 10.1016/0306-4522(96)00106-6.

Nolte, C. *et al.* (2001) 'GFAP Promoter-Controlled EGFP- Expressing Transgenic Mice : A Tool to Visualize Astrocytes and Astrogliosis in Living Brain Tissue', *Glia*, 33, pp. 72–86. doi: 10.1002/1098-1136(20010101)33:1<72::AID-GLIA1007>3.0.CO%3B2-A.

Northington, F. J. *et al.* (2001) 'Early neurodegeneration after hypoxia-ischemia in neonatal rat is necrosis while delayed neuronal death is apoptosis', *Neurobiology of Disease*, 8(2), pp. 207–219. doi: 10.1006/nbdi.2000.0371.

Northington, F. J., Chavez-Valdez, R. and Martin, L. J. (2011) 'Neuronal Cell Death in Neonatal Hypoxia-Ischemia', *Annals of Neurology*, 69(5), pp. 743–758. doi: 10.1002/ana.22419.Neuronal.

Oberheim, N. A. *et al.* (2010) 'Uniquely hominid features of adult human astrocytes', *Journal of Neurophysiology*, 29(10), p. 3276. doi: 10.1523/JNEUROSCI.4707-08.2009.Uniquely.

Ohashi, K. *et al.* (2018) 'TRPV4 is functionally expressed in oligodendrocyte precursor cells and increases their proliferation', *Pflugers Archiv European Journal of Physiology*, 470(5), pp. 705–716. doi: 10.1007/s00424-018-2130-3.

Olney, J. W. *et al.* (1986) 'The role of specific ions in glutamate neurotoxicity', *Neuroscience Letters*, 65(1), pp. 65–71. doi: 10.1016/0304-3940(86)90121-7.

Olney, J. W., Ho, O. L. and Rhee, V. (1971) 'Cytotoxic effects of acidic and sulphur containing amino acids on the infant mouse central nervous system', *Experimental Brain Research*, 14(1), pp. 61–76. doi: 10.1007/BF00234911.

Papadopoulos, M. C. and Verkman, A. S. (2005) 'Aquaporin-4 gene disruption in mice reduces brain swelling and mortality in pneumococcal meningitis', *Journal of Biological Chemistry*, 280(14), pp. 13906–13912. doi: 10.1074/jbc.M413627200.

Papadopoulos, M. C. and Verkman, A. S. (2013) 'Aquaporin water channels in the nervous system', *Nature Reviews Neuroscience*, 14(4), pp. 265–277. doi: 10.1038/nrn3468.

Parakalan, R. *et al.* (2012) 'Transcriptome analysis of amoeboid and ramified microglia isolated from the corpus callosum of rat brain', *BMC Neuroscience*, 13(1), p. 1. doi: 10.1186/1471-2202-13-64.

Parkhurst, C. N. *et al.* (2014) 'Microglia promote learning-dependent synapse formation through BDNF', *Cell*, 155(7), pp. 1596–1609. doi: 10.1016/j.cell.2013.11.030.Microglia.

Pascual, O. *et al.* (2012) 'Microglia activation triggers astrocyte-mediated modulation of excitatory neurotransmission', *Proceedings of the National Academy of Sciences of the United States of America*, 109(4), pp. E197–E205. doi: 10.1073/pnas.1111098109.

Pivonkova, H. *et al.* (2018) 'The Contribution of TRPV4 Channels to Astrocyte Volume Regulation 4 and Brain Edema Formation', *Neuroscience*, 394, pp. 127–143. doi: 10.1016/j.neuroscience.2018.10.028.

Preston, G. M. *et al.* (1992) 'Appearance of Water Channels in Xenopus Oocytes Expressing Red Cell CHIP28 Protein', *Science*, 256(5055), pp. 385–387. doi: 10.1126/science.256.5055.385.

Rakers, C., Schmid, M. and Petzold, G. C. (2017) 'TRPV4 channels contribute to calcium transients in astrocytes and neurons during peri-infarct depolarizations in a stroke model', *Glia*, 65(9), pp. 1550–1561. doi: 10.1002/glia.23183.

Ransom, B. R. and Blank, W. F. (1975) 'The pathology of cerebral edema', *Human Pathology*, 6(5), pp. 642–643. doi: 10.1016/S0046-8177(75)80054-2.

Rash, J. E. *et al.* (1998) 'Direct immunogold labeling of aquaporin-4 in square arrays of astrocyte and ependymocyte plasma membranes in rat brain and spinal cord.', *Proceedings of the National Academy of Sciences of the United States of America*, 95(20), pp. 11981–11986. doi: 10.1073/pnas.95.20.11981.

Risher, W. C., Andrew, R. D. and Kirov, S. A. (2009) 'Real-Time Passive Volume Responses of Astrocytes to Acute Osmotic and Ischemic Stress in Cortical Slices and in vivo Revealed by Two-Photon Microscopy', *Glia*, 57(2), pp. 207–221. doi: 10.1002/glia.20747.Real-Time.

Rosenberg, G. A. (1999) 'Ischemic brain edema', *Progress in Cardiovascular Diseases*, 42(3), pp. 209–216. doi: 10.1016/S0033-0620(99)70003-4.

Rossi, D. J., Oshima, T. and Attwell, D. (2000) 'Glutamate release in severe brain ischaemia is mainly by reversed uptake', *Nature*, 403(6767), pp. 316–321. doi: 10.1038/35002090.

Saadoun, S. *et al.* (2005) 'Involvement of aquaporin-4 in astroglial cell migration and glial scar formation', *Journal of Cell Science*, 118(24), pp. 5691–5698. doi: 10.1242/jcs.02680.

Sakers, K. *et al.* (2017) 'Astrocytes locally translate transcripts in their peripheral processes', *Proceedings of the National Academy of Sciences of the United States of America*, 114(19), pp. E3830–E3838. doi: 10.1073/pnas.1617782114.

Schuier, F. J. and Hossmann, K.-A. (1980) 'Experimental Brain Infarcts in Cats: II. Ischemic Brain Edema', *Stroke*, 11(6), pp. 593–601.

Shibasaki, K. *et al.* (2014) 'A novel subtype of astrocytes expressing TRPV4 (Transient Receptor Potential Vanilloid 4) Regulates neuronal excitability via release of gliotransmitters', *Journal of Biological Chemistry*, 289(21), pp. 14470–14480. doi: 10.1074/jbc.M114.557132.

Shigematsu, H. *et al.* (2010) 'A 3.5-nm structure of rat TRPV4 cation channel revealed by zernike phase-contrast cryoelectron microscopy', *Journal of Biological Chemistry*, 285(15), pp. 11210–11218. doi: 10.1074/jbc.M109.090712.

Smith, A. J. and Verkman, A. S. (2015) 'Superresolution Imaging of Aquaporin-4 Cluster Size in Antibody-Stained Paraffin Brain Sections', *Biophysical Journal*, 109(12), pp. 2511–2522. doi: 10.1016/j.bpj.2015.10.047.

Sofroniew, M. V. and Vinters, H. V. (2010) 'Astrocytes: Biology and pathology', *Acta Neuropathologica*, 119(1), pp. 7–35. doi: 10.1007/s00401-009-0619-8.

Sorbo, J. G. *et al.* (2008) 'The molecular composition of square arrays', *Biochemistry*, 47(8), pp. 2631–2637. doi: 10.1021/bi702146k.

Stelter, R. A. *et al.* (2014) 'Preconditioning Provides Neuroprotection in Models of CNS Disease: Paradigms and Clinical Significance', *Progress in Neurobiology*, 0, pp. 58–83. doi: 10.1016/j.pneurobio.2013.11.005.Preconditioning.

Tait, M. J. *et al.* (2008) 'Water movements in the brain: role of aquaporins', *Trends in Neurosciences*, 31(1), pp. 37–43. doi: 10.1016/j.tins.2007.11.003.

Takano, T. *et al.* (2006) 'Astrocyte-mediated control of cerebral blood flow', *Nature Neuroscience*, 9(2), pp. 260–267. doi: 10.1038/nn1623.

Tang, Y. *et al.* (2010) 'Effects of Aquaporin-4 on edema formation following intracerebral hemorrhage', *Experimental Neurology*. Elsevier Inc., 223(2), pp. 485–495. doi: 10.1016/j.expneurol.2010.01.015.

Tasca, C. I., Dal-Cim, T. and Cimarosti, H. (2015) 'In Vitro Oxygen-Glucose Deprivation to Study Ischemic Cell Death', *Methods in Molecular Biology*, 1254, pp. 197–210. doi: 10.1007/978-1-4939-2152-2_15.

Thomsen, R. *et al.* (2013) 'Alternative mRNA Splicing from the Glial Fibrillary Acidic Protein (GFAP) Gene Generates Isoforms with Distinct Subcellular mRNA Localization Patterns in Astrocytes', *PLoS ONE*, 8(8). doi: 10.1371/journal.pone.0072110.

Tornabene, E. and Brodin, B. (2016) 'Stroke and Drug Delivery - In Vitro Models of the Ischemic Blood-Brain Barrier', *Journal of Pharmaceutical Sciences*. Elsevier Ltd, 105(2), pp. 398–405. doi: 10.1016/j.xphs.2015.11.041.

Torp, R. *et al.* (1991) 'Cellular and subcellular redistribution of glutamate-, glutamine- and taurine-like inmunoreactivities during forebrain ischemia: a semiquantitative electron microscopic study in rat hippocampus', *Neuroscience*, 41(2/3), pp. 433–447. doi: 10.1016/0306-4522(91)90339-P

Tress, O. *et al.* (2012) 'Panglial Gap Junctional Communication is Essential for Maintenance of Myelin in the CNS', *Journal of Neuroscience*, 32(22), pp. 7499–7518. doi: 10.1523/JNEUROSCI.0392-12.2012.

Ueno, M. *et al.* (2013) 'Layer v cortical neurons require microglial support for survival during postnatal development', *Nature Neuroscience*. Nature Publishing Group, 16(5), pp. 543–551. doi: 10.1038/nn.3358.

Unger, V. M. *et al.* (1999) 'Three-dimensional structure of a recombinant gap junction membrane channel.', *Science*, 283(5405), pp. 1176–1180. doi: 10.1126/science.283.5405.1176.

Unterberg, A. W. *et al.* (2004) 'Edema and brain trauma', *Neuroscience*, 129, pp. 1021–1029. doi: 10.1016/j.neuroscience.2004.06.046.

Watanabe, H. *et al.* (2002) 'Heat-evoked activation of TRPV4 channels in a HEK293 cell expression system and in native mouse aorta endothelial cells', *Journal of Biological Chemistry*, 277(49), pp. 47044–47051. doi: 10.1074/jbc.M208277200.

Witthoft, A., Filosa, J. A. and Karniadakis, G. E. (2013) 'Potassium buffering in the neurovascular unit: Models and sensitivity analysis', *Biophysical Journal*. Biophysical Society, 105(9), pp. 2046–2054. doi: 10.1016/j.bpj.2013.09.012.

Woodruff, T. M. *et al.* (2011) 'Pathophysiology, treatment, and animal and cellular models of human ischemic stroke', *Molecular Neurodegeneration*. BioMed Central Ltd, 6(1), p. 11. doi: 10.1186/1750-1326-6-11.

Wu, L., Yu, X. and Feng, L. (2015) 'Connexin 43 stabilizes astrocytes in a stroke-like milieu to facilitate neuronal recovery', *Acta Pharmacologica Sinica*, (36), pp. 928–938. doi: 10.1038/aps.2015.39.

Xie, H. *et al.* (2017) 'Evaluation of Connexin 43 Redistribution and Endocytosis in Astrocytes Subjected to Ischemia / Reperfusion or Oxygen-Glucose Deprivation and Reoxygenation', *BioMed research international*. Hindawi, 2017, p. 5064683. doi: 10.1155/2017/5064683.

Yang, Y., Lewis, R. and Miller, R. H. (2011) 'Interactions between oligodendrocyte precursors control the onset of CNS myelination', *Developmental Biology*, 350(1), pp. 127–138. doi: 10.1021/nn300902w.Release.

Yao, X. *et al.* (2015) 'Reduced brain edema and infarct volume in aquaporin-4 deficient mice after transient focal cerebral ischemia', *Neuroscience Letters*, (584), pp. 368–372. doi: 10.1016/j.neulet.2014.10.040.Reduced.

Zamanian, J. L. J. *et al.* (2012) 'Genomic Analysis of Reactive Astrogliosis', *The Journal of Neuroscience*, 32(18), pp. 6391–6410. doi: 10.1523/JNEUROSCI.6221-11.2012.Genomic.

Zhang, H. and Verkman, A. S. (2008) 'Aquaporin-4 Independent Kir4.1 K+ Channel Function in Brain Glial Cells', *Molecular and Cellular Neuroscience*, 37(1), pp. 1–10. doi: 10.1016/j.mcn.2007.08.007.

Zonta, M. *et al.* (2003) 'Neuron-to-astrocyte signaling is central to the dynamic control of brain microcirculation', *Nature Neuroscience*, 6(1), pp. 43–50. doi: 10.1038/nn980.